https://doi.org/10.5194/egusphere-2026-3778
Preprint. Discussion started: 8 July 2026


# Size-resolved characterizations of Fe in aerosols in East Asian outflow in winter and spring: Source apportionment and bioaccessibility

Takuma Miyakawa[1], Chunmao Zhu[1], Morihisa Yokokawa[2], Mitsunobu Mukawa[3], Akinori Ito[1], Atsushi Shimizu[4], Tomoaki Nishizawa[4], and Yugo Kanaya[1]

[1]Research Institute for Global Change, Japan Agency for Marine-Earth Science and Technology (JAMSTEC), Yokohama, 236-0001, Japan

[2]Sibata Scientific Technology Ltd., Soka, 340-0005, Japan
[3]Murata Keisokuki Service Co., Ltd., Yokohama, 245-0052, Japan
[4]National Institute for Environmental Studies, Tsukuba, 305-8506, Japan

*Correspondence to*: Takuma Miyakawa (miyakawat@jamstec.go.jp)

**Abstract.**

Trace metals in aerosol particles affect the Earth's radiative budget, human health, and ocean biogeochemistry. Semi-continuous measurements of the elemental composition of fine-mode ($PM_{2.5}$) and total ($PM_{10}$) aerosols and high-volume air sampling (5-d)/offline chemical analyses were conducted on a remote island of Japan in winter–spring 2023–2024 to characterize the source apportionment and water-soluble (i.e., bioaccessible) concentrations/fractions of trace elements such as Fe in the East Asian outflow region. Temporal variations in $PM_{2.5}$ and $PM_{10}$ Fe concentrations were classified into dust and non-dust contributions based on multilinear regression using concentrations of tracer species. Size-segregated water-soluble Fe fraction ($f_{Fe,sol}$) was investigated using dust Fe contributions and aging processes (e.g., transport time). Source apportionment (dust vs. non-dust) was essential to account for $f_{Fe,sol}$ variations for $PM_{2.5}$ aerosols, whereas those for coarse-mode aerosols were largely affected by aging processes. Temporal variations in total water-soluble Fe ($Fe_{sol}$) concentrations were strongly correlated with black carbon (BC) concentrations, indicating the role of continental combustion sources in enhancing $Fe_{sol}$ concentrations in the outflow regions. The enhancement ratios of $Fe_{sol}$ to BC concentrations were 53.8 (±11) ng $\mu g^{-1}$ on average during the observation period and increased from ~40 ng $\mu g^{-1}$ in winter to ~90 ng $\mu g^{-1}$ in spring. This may reflect increased dust contributions to $Fe_{sol}$ and reduced BC emissions from residential sector, as indicated by model analyses. These offer useful constraints for developing, validating, and refining numerical models of aerosol Fe behavior in the East Asian outflow.

https://doi.org/10.5194/egusphere-2026-3778
Preprint. Discussion started: 8 July 2026


## 1 Introduction

Atmospheric iron (Fe) in aerosol particles has attracted considerable attention because of its multiple effects on climate, air quality, human health, and marine biogeochemical cycles (e.g., Al-Abadleh et al., 2023; Jickells et al., 2005). Iron is one of the most abundant transition metals in atmospheric aerosols and is supplied to the atmosphere from both natural and anthropogenic sources, including emissions from mineral dust, biomass burning, coal combustion, industrial activities, and shipping. The relative importance of these sources varies spatially and seasonally, particularly in regions strongly affected by continental outflow (Ito et al., 2023; Mahowald et al., 2018).

From a climate perspective, Fe-containing aerosols influence the Earth's radiative balance directly and indirectly. Dust particles containing Fe-bearing minerals absorb and scatter solar and longwave radiation (Tegen and Lacis, 1996) and play a significant role in cloud formation (Nenes et al., 2014), leading to a large impact on the Earth's radiative budget (e.g., Di Biagio et al., 2020; Karydis et al., 2011; McCoy et al., 2017). Anthropogenic iron oxides ($FeO_X$) (e.g., magnetite) particles efficiently absorb solar radiation and have a significant impact on regional radiative forcing (Ito et al., 2021; Lamb et al., 2021; Moteki et al., 2017). In addition, Fe can participate in aerosol-phase chemical reactions that form secondary aerosols (e.g., Brandt and van Eldik, 1995), contributing to uncertainties in aerosol radiative forcing estimates in current climate models. Fe is also important in public health because transition metals such as Fe, Cu, and Ni can catalyze the *in vivo* formation of reactive oxygen species through redox cycling reactions (Charrier and Anastasio, 2012). Water-soluble Fe in fine aerosol particles may enhance oxidative stress in the human respiratory system and has been linked to adverse health effects associated with $PM_{2.5}$ exposure (Lakey et al., 2016). Therefore, both total Fe concentration and the water-soluble Fe fraction are important for evaluating aerosol toxicity. Furthermore, the atmospheric deposition of Fe plays a critical role in marine ecosystems (Tagliabue et al., 2017). In many oceanic regions, especially high-nutrient low-chlorophyll (HNLC) regions such as the Northwestern Pacific Ocean (NWPO) and Southern Ocean (Basterretxea et al., 2023), bioavailable Fe is a limiting micronutrient for phytoplankton growth. Aerosol deposition supplies externally derived Fe to the ocean surface and stimulates marine primary productivity and carbon uptake. Bioavailability represents the fraction of Fe that marine biota can immediately uptake and use under realistic oceanic conditions. Bioaccessibile Fe refers to labile Fe in aerosol water and becomes available for biological uptake under environmentally relevant conditions (i.e., potentially bioavailable) whereas water-soluble Fe refers to Fe released into water measured through the defined extraction method (Meskhidze et al., 2026). Because water-soluble Fe is more bioavailable than insoluble forms (e.g., crystalline $FeO_X$ in dust particles), water-soluble Fe is regarded as a proxy of bioaccessible Fe in this study. Although only a small fraction of total aerosol Fe is water-soluble (e.g., Sholkovitz et al., 2012), the fractional solubility of Fe varies substantially depending on the aerosol source, atmospheric processing such as acidification, and cloud processing during long-range transport (e.g., Ito et al., 2020; Mahowald et al., 2018). Quantitative investigations of the variations in the fractional solubility of Fe and its controlling factors are urgently needed to understand the diverse roles of Fe-containing aerosols in the Earth's environment.

https://doi.org/10.5194/egusphere-2026-3778
Preprint. Discussion started: 8 July 2026


East Asia is one of the largest source regions of atmospheric aerosols, including metallic elements (Pacyna and Pacyna, 2001), emitting large amounts of both mineral dust (i.e., Asian dust) and anthropogenic combustion-derived particles (e.g., Myhre et al., 2013). During the East Asian winter monsoon season, these aerosols are efficiently transported to the downwind regions of the continent (e.g., Japan) and the NWPO. Asian dust aerosols are typically enriched in total Fe but exhibit low solubility, whereas anthropogenic aerosols often contain less Fe but show substantially higher solubility due to atmospheric processing (e.g., Kurisu et al., 2021). Consequently, distinguishing dust and non-dust Fe contributions and understanding the evolution of Fe solubility (bioaccessibility) during transport are essential for accurately assessing the environmental impact of East Asian outflow aerosols. We deployed the Integrated Massively Parallel Atmospheric Chemical Transport Model (IMPACT; e.g., Ito et al., 2023) to accurately simulate Fe aerosol concentrations and variations in their bioaccessibility by considering a detailed chemical aging process, thereby improving the role of Fe in the Earth system. Recently, the IMPACT model was refined to simulate the multi-elemental compositions of atmospheric aerosols (Ito and Miyakawa et al., 2023; Miyakawa et al., 2023), and it has been evaluated and updated in terms of source apportionment, bioaccessibility, and removal processes of Fe in East Asian outflow using high-temporal resolution measurements of Fe in fine aerosols and tracer compounds (Miyakawa et al., 2023) and size-resolved (fine and coarse) characterizations of stable isotope ratios of aerosol Fe and water-soluble Fe (Kurisu et al., 2026).

Despite the importance of aerosol Fe, observational constraints on the temporal variability, source apportionment, and size-dependent solubility of aerosol Fe remain limited, especially with continuous measurements in remote outflow regions. Simultaneous observations of the concentrations and fractional solubility of fine- and coarse-aerosol Fe are necessary to improve our understanding of Fe cycling in the atmosphere and refine numerical models describing aerosol chemistry and ocean nutrient supply. In this study, we conducted semi-continuous elemental measurements of $PM_{2.5}$ and $PM_{10}$ aerosols using a newly developed system integrating an aerosol elemental analyzer which has been deployed in our previous studies (Miyakawa et al., 2023; 2025), together with high-volume aerosol sampling and offline chemical analyses, on a remote island in Japan during the winter–spring period of 2023–2024. The objectives of this study were (1) to characterize temporal variations in total and water-soluble Fe concentrations, (2) to distinguish dust and non-dust contributions using tracer-based source apportionment, and (3) to investigate the relationships among Fe solubility, particle size, and atmospheric aging processes under the influence of East Asian outflow. The datasets were validated with independent measurements and used to evaluate and analyze the IMPACT-model simulations. These findings provide useful observational constraints for improving atmospheric chemical transport models and understanding aerosol roles in regional climate and marine biogeochemistry.

## 2 Material and methods

### 2.1 Atmospheric aerosol observations and sampling at Fukue Island

Continuous measurements of trace gases and $PM_{2.5}$ aerosols have been conducted on Fukue Island, a remote island in western Japan, since February 2009 (Kanaya et al., 2016; Miyakawa et al., 2023). The observation site (Fukue site), the Fukue Island

https://doi.org/10.5194/egusphere-2026-3778
Preprint. Discussion started: 8 July 2026


Atmospheric Environment Monitoring Station (32.75° N, 128.68° E), was located at the northwestern part of the island. The mass concentrations of fine particles ($PM_{2.5}$) were measured using a Synchronized Hybrid Ambient Real-time Particulate (SHARP) monitor (model 5030, Thermo Fisher Scientific, Inc., USA) (Kanaya et al., 2016). Black carbon (BC) mass concentrations were measured using a Continuous Soot Monitoring System (COSMOS, model 3130, Kanomax Corp., JP) and a Multi Angle Absorption Photometer (MAAP, model 5012, Thermo Scientific, Inc., USA). According to intercomparison studies between the MAAP and other independent instruments (Kanaya et al., 2013; 2016; Miyakawa et al., 2019), the mass absorption cross-section for the MAAP was modified from the manufacturer's recommendation of 6.6 to 10.3 $m^2 g^{-1}$. BC observations using MAAP and COSMOS were evaluated using a Single Particle Soot Photometer (Droplet Measurement Technologies, Colorado, USA) (Miyakawa et al., 2017; 2019). Based on the above evaluations, Kanaya et al. (2020) unified BC concentration records from MAAP and COSMOS to minimize data gaps caused by failures in individual measurements. In this study, we used a "unified" dataset of BC concentrations. Details of the $PM_{2.5}$ and BC measurements are outlined in Kanaya et al. (2016; 2020), which revealed that the elevated $PM_{2.5}$ and BC concentrations at the observation site were mainly affected by the transboundary transport of polluted air masses from the Asian continent (i.e., long-range transport) with a negligible impact from local emission sources (e.g., Kanaya et al., 2016).

The elemental compositions of $PM_{2.5}$ and $PM_{10}$ aerosols were measured using a Continuous Particulate Monitor with X-ray Fluorescence (XRF) analysis (PX-375, Horiba Ltd., Kyoto, Japan). The basic information on the instrumental design is described in Asano et al. (2017) and Miyakawa et al. (2023; 2025). However, the instrument can be briefly described as follows: PX-375 consists of a collection unit for aerosol particles on a filter, a measurement unit for the mass of the collected aerosol particles, and an XRF analysis chamber; the filter tape used for particle collection was fabricated by Horiba Ltd. (TFH-01, Horiba Ltd.); and TFH-01 is a polytetrafluoroethylene filter with non-woven fabric polyethylene and polyethylene terephthalate backing, which was designed to mechanically strengthen the filter structure. The total aerosol mass collected on the filter was analyzed using a radiocarbon-based beta-ray attenuation method during particle collection. After sampling, a particle-laden spot on the filter was transferred into the XRF analysis chamber by advancing the filter roll tape and then analyzed based on XRF. During the observation period, aerosol particles were collected for 4 h, and XRF analyses were performed with 4000 s of X-ray irradiation at 15 and 50 kV. The typical volume of the sampled air was 4 $m^3$ per particle-laden spot. The limits of detection (LODs) were evaluated by repeated measurements placing the high-efficiency particulate air filter in front of the PX-375 to introduce particle-free air into the PX-375. The LODs were defined as three times the standard deviations of the measured values by the PX-375 at the observation site and were evaluated to be 1.07, 0.07, 0.08, 0.16, 0.33, 1.28, 4.26, 4.80, 1.75, 0.36, 0.07, 0.10, 0.26, and 0.35 ng $m^{-3}$ for Fe, Ni, Cu, Zn, As, Si, S as sulfate, K, Ca, Ti, V, Cr, Mn, and Pb, respectively. The particle-laden spots on the filter roll tape were cut into pieces after the observation period and stored in a refrigerator (at approximately −20 °C). Particle spots can be reanalyzed using different techniques (e.g., Miyakawa et al., 2023; 2025; Zhu et al., 2021). In this study, particle spots collected during the observations were reanalyzed for calibrations using ambient aerosols with different chemical analyses: ion chromatography (IC) for S (as sulfate) and Inductively Coupled Plasma Mass Spectrometry (ICP-MS) for Ti, V, Fe, Mn, Ni, Cu, Zn, As, and Pb (Miyakawa et al., 2025).

https://doi.org/10.5194/egusphere-2026-3778
Preprint. Discussion started: 8 July 2026


We placed PX-375 in a newly developed shelter (**Figs. S1**) on the rooftop of the observation container at Fukue site. The shelter had two sampling lines for collecting $PM_{2.5}$ and $PM_{10}$ aerosols, which were alternately changed in conjunction with the operation of the PX-375 pump. A $PM_{2.5}$ very sharp cut cyclone (VSCC, Mesa Lab. Inc., Colorado, USA) and EPA Louvered $PM_{10}$ impactor (SSI2.5, Mesa Lab. Inc., Colorado, USA) were used in this study. The specification and performance of the measurement system were described in **Section S1**.

Fine and coarse aerosol particles were collected using a high-volume air sampler (HVS; HV-120SL, Kimoto Electric, Ltd., Osaka, Japan) with a single-stage impactor (TE-231, Tisch Environmental, Inc., Ohio, USA). Air sampling was conducted for approximately 5 days on an 8 × 10-inch pre-combusted (900 °C for 3 h) quartz fiber filter (PALLFLEX TISSUQUARTZ 2500QAT-UP, Pall Corp., New York, USA) for fine-mode ($PM_{2.5}$) particles. We also used a pre-combusted quartz fiber filter with slits (TE-230-QZ, Tisch Environmental, Inc.) on the impaction plate of the TE-231 to collect coarse-mode (>2.5 μm in aerodynamic diameter) particles. For the evaluations of $PM_{10}$ aerosol elemental compositions by PX-375, the analyzed concentrations of $PM_{2.5}$ and coarse-mode samples collected by the HVS were integrated to derive the total concentrations of element X ($[X]_{tot} = [X]_{fine} + [X]_{coarse}$). The filter samples were stored at −20 °C until further analysis. The sampling log is summarized in **Table S1**.

Lidar-derived aerosol extinction coefficients at 532 nm (e.g., Shimizu et al., 2016) were analyzed to investigate the impact of Asian dust on the measured aerosol concentrations. The lidar measurements at the same site were part of the lidar network in Asia and were maintained by the National Institute for Environmental Studies in Japan (Shimizu et al., 2004; Sugimoto et al., 2003). The contribution of dust to the lidar-derived aerosol extinction coefficient was estimated using the aerosol depolarization ratio, assuming that dust particles were externally mixed with spherical particles. All lidar data were obtained with 15 min temporal and 30 m vertical resolutions. Near-surface dust and total aerosol extinction coefficients were estimated by averaging the corresponding extinction coefficients between 120 and 240 m; measurements below 120 m were unavailable and therefore omitted. The resulting values were then merged with the 4-hourly elemental composition datasets.

### 2.2 Aerosol sampling near anthropogenic emissions in Japan

Ground-based aerosol sampling was performed from October 17 to November 21, 2022, at the Japan Agency for Marine-Earth Science and Technology campus (35.32N, 139.65E, ~10 m ASL) (Yokosuka site), located in an industrialized region along the Tokyo Bay, ~30 km south of the Tokyo metropolitan center (Miyakawa et al., 2016; 2020). Fine and coarse aerosol particles were collected using the same setup as the sampler and filters at the Fukue site. Air sampling was conducted for 2–3 days per each sample. As the air masses observed at the Yokosuka site are not strongly affected by local emissions and are representative of mixtures of those affected by multiple sources in the industrialized region (Miyakawa et al., 2020), the collected samples from this site were analyzed to investigate the levels and variations in the concentrations and fractional solubility of Fe near anthropogenic emission sources in Japan. The sampling log is summarized in **Table S2**.

https://doi.org/10.5194/egusphere-2026-3778
Preprint. Discussion started: 8 July 2026


### 2.3 Chemical analyses

In this study, we analyzed the fine- ($PM_{2.5}$) and coarse-mode aerosol chemical compositions. Chemical analyses of inorganic compounds (ions) and trace metals were conducted at Murata Keisokuki Service Co., Ltd. (Kanagawa, Japan). Thermal–optical analyses were conducted to quantify the mass concentrations of elemental carbon (EC) and organic carbon (OC) using a carbon analyzer (DRI model 2001; Desert Research Institute, Nevada, USA). The modified interagency monitoring of protected visual environments (IMPROVE_A; Chow et al. 2007) temperature protocol with the thermal-optical reflectance (TOR) measurements was used for the analyses. A filter aliquot was separated into a 1 × 1-cm piece for fine-mode and a slit for coarse-mode particles to analyze the water-soluble ions. Water-soluble ions—ammonium ($NH_4^+$), sodium ($Na^+$), potassium ($K^+$), calcium ($Ca^{2+}$), magnesium ($Mg^{2+}$), sulfate ($SO_4^{2-}$), nitrate ($NO_3^-$), and chloride ($Cl^-$)—in fine mode aerosols were analyzed using IC (Dionex ICS1000, Thermo Fisher Scientific K.K., Tokyo, Japan) for the validation of S measurements using the PX-375. The total and water-soluble metals in fine- and coarse-mode aerosols were analyzed using ICP-MS (7700X, Agilent Technologies, Inc., US). The acid digestion method was used to quantify the total metal concentrations (Miyakawa et al., 2019). A comparison between these offline analyses and online measurements using PX-375 will be discussed later. Further to the analysis of total metal masses, a leaching method using ultrapure water, as described by Buck et al. (2006), was applied to analyze water-soluble (bioaccessible) metal concentrations.

### 2.4 Meteorological and satellite data analyses

Backward trajectories were calculated from the observation site to elucidate the impact of Asian outflows. Five-day backward trajectories from the observation site (at a starting altitude of 0.5 km) were calculated every hour using the NOAA Hybrid Single-Particle Lagrangian Integrated Trajectory Model (Stein et al., 2015) with meteorological datasets at a resolution of 1° in latitude and longitude (NCEP's Global Data Assimilation System (GDAS1)). The accumulated precipitation along the trajectories (APT) for three days before the measurement was calculated to discuss wet removal during transport (Kanaya et al., 2016; Miyakawa et al., 2017; 2023). The relative humidity averaged for a day before the observations ($RH_{-1d}$) and at the time of observations ($RH_t$) were also analyzed to investigate the impacts of liquid-phase processes (including cloud processing) during the transport and hygroscopic growth of aerosols, respectively.

The daily mean aerosol optical depth (AOD) at a wavelength of 550 nm ($AOD_{550}$) measured by the Moderate Resolution Imaging Spectrometer (MODIS) aboard the Aqua satellite was analyzed to investigate the spatial distribution of aerosols over East Asia. $AOD_{550}$ was retrieved using the dark target (DT) and deep blue (DB) algorithms (Sayer et al. 2014). We used the final product, called MODIS-Aqua Combined DT and DB AOD at 550 nm for land and ocean (MYD08_M3_v6.1).

https://doi.org/10.5194/egusphere-2026-3778
Preprint. Discussion started: 8 July 2026


### 2.5 Integrated Massively Parallel Atmospheric Chemical Transport Model

In this study, the IMPACT model (Ito and Miyakawa, 2023; Kurisu et al., 2026; Miyakawa et al., 2023; Ito et al., in preparation) was deployed to simulate the three-dimensional distribution of atmospheric composition, including targeted aerosol species/elements such as Fe. Ito and Miyakawa (2023) and Miyakawa et al. (2023) modified anthropogenic Fe emission sources by including metal smelting and expanded its capability to simulate elements other than Fe (e.g., Si, Mn, Cu, and Pb). Kurisu et al. (2026) further modified anthropogenic Fe emission sources beyond smelting processes, leading to increased aerosol Fe content from the road transport and railway sectors (Dubois et al., 2025). The simulated total and water-soluble Fe concentrations were compared with the observations of this study. Source apportionment of Fe in $PM_{2.5}$, $PM_5$, and $PM_{20}$ aerosols was also analyzed based on the tagged tracer simulations using the IMPACT model, which can separately simulate lithogenic (i.e., mineral dust), pyrogenic (i.e., biomass burning), and sector-resolved anthropogenic contributions of Fe to $PM_{2.5}$, $PM_5$, and $PM_{20}$. A brief description of the IMPACT model is described as follows.

The model simulations were performed using a horizontal resolution of 2.0° × 2.5° (latitude × longitude) and 47 vertical layers. An emission inventory, Community Emissions Data System (CEDS, v-2025-04-18, Hosely et al., 2025), was used for fine particulate matter and BC emitted from anthropogenic sources. The metal content of $PM_{2.5}$ aerosols from lithogenic, pyrogenic, and anthropogenic sources was obtained by compiling source-specific aerosol measurements (Ito and Miyakawa, 2023; Dubois et al., 2025; Li et al., 2026). The IMPACT model simulated wet removal processes through in-cloud (e.g., Ito and Xu, 2014) and below-cloud scavenging (Ito and Kok, 2017) processes. In the model simulations, all the metal components for pyrogenic and anthropogenic aerosols in the smallest size bin were removed at the same rates as BC from pyrogenic and anthropogenic sources, respectively, assuming internal mixing of BC and trace elements; thus, removal efficiencies did not differ among elements in anthropogenic aerosols in the smallest size bin (e.g., Ito and Feng, 2010).

## 3 Results and discussion

### 3.1 Evaluations of the online measurements of trace elements in $PM_{2.5}$ and $PM_{10}$ aerosols

#### 3.1.1 Comparison with the different measurements using collocated instruments

We evaluated the online measurements of total, elemental, and BC concentrations of $PM_{2.5}$ and $PM_{10}$ aerosols using PX-375 and MAAP/COSMOS with collocated instruments (SHARP) with offline chemical analyses of the filter samples collected by the HVS with a $PM_{2.5}$ impactor (**Figs. S3–S4**). The $PM_{2.5}$ mass concentrations measured using PX-375 were compared with those measured using the SHARP monitor. The results were in good agreement (within ~30 %) (**Fig. S3a**). The MAAP/COSMOS-derived unified BC concentrations were well correlated ($r^2 = 0.91$) with the EC mass concentrations from thermal-optical analyses of the filters collected by the HVS (**Fig. S3b**). The EC mass concentrations were systematically higher than the BC concentrations because of the uncertainties related to the temperature-rising protocols and the charring corrections in the thermal-optical analyses (Chow et al., 2001; Miyakawa et al., 2016). In this study, we used BC data (not EC) to investigate

https://doi.org/10.5194/egusphere-2026-3778
Preprint. Discussion started: 8 July 2026


the impacts of combustion sources in the East Asian continental region. Sulfate concentrations were calculated using sulfur element concentrations measured using PX-375, assuming that all sulfur elements existed as sulfate. **Figure S3c** shows a comparison of sulfate concentrations between PX-375 and the chemical analyses of the HVS samples. These were in good agreement (within ~30 %) and had good correlations ($r^2$ = 0.89).

The elemental characterization of $PM_{2.5}$ and $PM_{10}$ aerosols using PX-375 was evaluated by comparing the chemical analyses of HVS samples. The intercomparison results for the elemental characterizations of PX-375 and HVS are shown in **Fig. S4**. In general, PX-375-derived $PM_{10}$ concentrations for almost all elements (except Cr and Pb) agreed well (<±30 %) with HVS-derived total concentrations, even though the size cut definition was different between the two methods ($PM_{10}$ vs. fine + coarse). The comparison of $PM_{2.5}$ concentrations indicated some biases in PX-375 relative to HVS. These agreements indicate that the quantification of elemental concentrations by PX-375 was reasonable; however, differences in the size-cut performance of the two instruments may affect the comparison results. The $PM_{2.5}/PM_{10}$ elemental mass ratios for PX-375 were compared with the fine mode mass fraction for HVS and showed positive biases for the elements (e.g., Ca, Fe, and Ti) with smaller $PM_{2.5}/PM_{10}$ ratios (**Fig. S5**). As coarse-mode particles significantly contributed to the total masses for such elements, the partitioning of masses between fine and coarse modes and the contributions of particles larger than 10 μm in aerodynamic diameter affected the biases shown in the comparison. The partitioning can be affected by the differences in the accuracy of the designed particle diameters, with 50 % efficiency of the particle collection and the steepness of the particle collection efficiency as a function of particle diameter between the size-separating devices (the Tisch impactor for HVS (e.g., Willeke, 1975) vs. VSCC for PX-375 (e.g., Kenny et al., 2004)). Interstage aerosol losses and the lower collection efficiency for accumulation-mode particles in the impactor used for HVS (Howell et al., 1998) were additional sources of uncertainty in the HVS-derived results. Although this result alone does not allow the relative contributions of these factors to the observed biases to be determined, uncertainties related to the performance of the impactor used for HVS are likely considered more significant, as discussed in the following section (section 3.1.2).

### 3.1.2 Spatial representativeness of the online measurements of $PM_{2.5}$ and $PM_{10}$ aerosols at the observation site

$PM_{2.5}$ and $PM_{10}$ mass concentrations measured using the PX-375 were compared with those measured at a different site (32.70° N, 128.84° E ~16 km east of our site) on Fukue Island, which is one of the observation sites of the Atmospheric Environmental Observation System (AEROS) managed by the Ministry of Environment, Japan (MoEJ). Our measurements of $PM_{2.5}$ and $PM_{10}$ aerosol mass concentrations were 20–30 % biased to AEROS observations of $PM_{2.5}$ and Suspended Particulate Matter (SPM) concentrations but showed higher correlation coefficients ($r^2$ = ~0.85) (**Figs. S6a–S6b**). As SPM corresponded approximately to $PM_7$ rather than $PM_{10}$, differences in the size cut likely contributed to the bias in $PM_{10}$ concentrations at our site. Mass concentrations of the key elements (Si, Ti, V, Mn, Fe, Ni, Cu, Zn, As, and Pb) and chemical compositions (sulfate and BC) in $PM_{2.5}$ aerosols at our site were compared with those measured from daily sampling using a low-volume air sampler (LVS) with a slit-jet $PM_{2.5}$ impactor (Murata Keisokuki Service, Co. Ltd., Japan) for January 18 to February 1, 2024, and the following

https://doi.org/10.5194/egusphere-2026-3778
Preprint. Discussion started: 8 July 2026


chemical analyses at a different site, Tamanoura (32.61° N, 128.66° E ~16.5 km south from our site) in Fukue Island, which is also a part of the atmospheric environmental monitoring activities led by MoEJ. Although measurements/sampling time resolutions and site locations differed, the levels and temporal variations of most components, except Si and BC, reasonably agreed well between the two sites, within ±30 % (**Table S3 and Fig. S7**). These results suggest that the measurements of $PM_{2.5}$ and $PM_{10}$ aerosols at our site were not substantially affected by local aerosol sources and provided spatially representative results to a great extent, as indicated in our previous studies (e.g., Kanaya et al., 2016). The difference in mass concentrations between BC and EC can be attributed to methodological differences between light absorption measurements vs. thermal-optical analysis, as also observed in the onsite comparison between BC and EC described in Section 3.1.1. Measurements for Si quantification using PX-375 were not rigorously calibrated using ambient samples (see Section 2.1). We then evaluated the uncertainties in the Si concentrations to be approximately 60 %.

The size-cut performance of the slit-jet $PM_{2.5}$ impactor used for the LVS was evaluated by the manufacturer to be equivalent to that of the Federal Reference Method $PM_{2.5}$ impactor (e.g., "Well Impactor Ninety-Six (WINS)") (https://www.murata-s.co.jp/wp/wp-content/uploads/2020/09/MCAS-SJ.pdf). The VSCC used for PX-375 has a precise size cut at 2.5 μm and steepness as good as WINS (Kenny et al., 2004). The reasonable agreement in the $PM_{2.5}$ elemental concentrations between the LVS and HVS suggests that the uncertainty of the size cut performance suggested in the comparison between PX-375 and HVS (see Section 3.1.1) can be attributed to the performance of the impactor used for HVS.

### 3.2 Variations in concentrations of $PM_{2.5}$ and $PM_{10}$ aerosols in the East Asian outflow

The temporal variations in the total, Si, and sulfate mass concentrations in $PM_{2.5}$ and $PM_{10}$ aerosols and BC mass concentrations are shown in **Figs. 1 and S8**. The average concentrations of total mass, Si, and sulfate for $PM_{2.5}$ ($PM_{10}$) aerosols and BC were 11.8 μg $m^{-3}$ (16.3 μg $m^{-3}$), 0.38 μg $m^{-3}$ (0.80 μg $m^{-3}$), 2.47 μg $m^{-3}$ (2.65 μg $m^{-3}$), and 0.18 μg $m^{-3}$, respectively, on average during the observation period. Si aerosols showed significant differences in mass concentrations among the size cuts ($PM_{2.5}$ and $PM_{10}$), whereas sulfate did not. The differences in size distributions among the elements (mineral dust vs. secondary aerosol) likely account for this feature. The concentrations of all components varied significantly during the observation period, with the total aerosol mass concentration peaking in mid-April 2024 (April 18–20, 2024). The concurrent increase in Si concentrations indicates the influence of Asian dust transport at the site. In contrast, BC and sulfate mass concentrations peaked in mid-February 2024 (February 11, 2024) without large enhancements of the Si mass concentrations, suggesting dominant continental anthropogenic influences. It was found that total $PM_{2.5}$ aerosol concentrations exceeded the short-term air quality standard (daily concentrations > 35 μg $m^{-3}$) in Japan during two elevated aerosol concentration events with a different cause (dust vs. anthropogenic). The satellite-derived spatial distributions of $AOD_{550}$ and backward trajectories for February 10–17, 2024, and April 15-22, 2024, are shown in **Fig. 2**. The extreme event of Si concentration elevation (April 18–20, 2024) was associated with air mass transport from northeast China and a high $AOD_{550}$ distribution widely spread over the north and northeast China region and the Sea of Japan. This suggests that the concentrations at the observation site were affected by

https://doi.org/10.5194/egusphere-2026-3778
Preprint. Discussion started: 8 July 2026


large-scale dust-storm transport from the source region (e.g., Gobi Desert) to the East Asian outflow regions. The event in mid-February 2024 was characterized by rapid changes in BC and sulfate concentrations within a short period (i.e., ~1 d), consistent with rapid air-mass transport from densely populated regions (e.g., Qingdao) in east-central China. High temporal-resolution variations in Fe mass concentrations in $PM_{2.5}$ and $PM_{10}$ aerosols are shown in **Fig. 3**. The average concentrations of Fe in $PM_{2.5}$ and $PM_{10}$ aerosols were 0.12 (±0.31) and 0.27 (±0.84) μg $m^{-3}$, respectively. Similar to Si, the mass contributions in the size range of 2.5–10 μm in aerodynamic diameter were significant for Fe during the observation period, owing to the dominant contribution of dust to Fe mass.

https://doi.org/10.5194/egusphere-2026-3778
Preprint. Discussion started: 8 July 2026


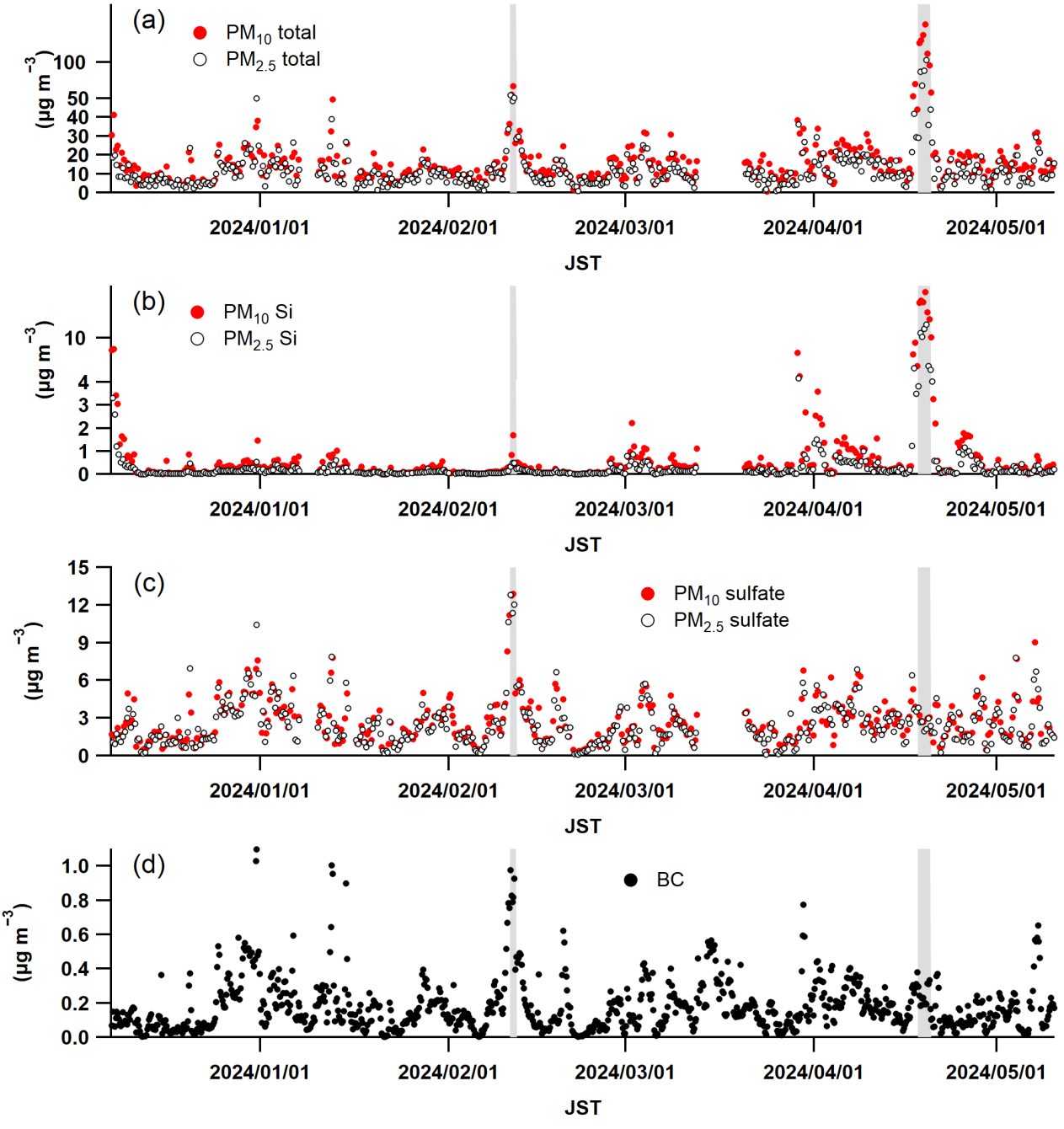


295 **Figure 1. Temporal variations in the concentrations of (a) $PM_{10}$ (red circles) and $PM_{2.5}$ (open circles) total mass, (b) $PM_{10}$ (red circles) and $PM_{2.5}$ (open circles) Si, (c) $PM_{10}$ (red circles) and $PM_{2.5}$ (open circles) sulfate, and (d) black**

https://doi.org/10.5194/egusphere-2026-3778
Preprint. Discussion started: 8 July 2026


**carbon (BC) during the observation period. The periods when the Japanese short-term air quality standard for $PM_{2.5}$ was exceeded (daily $PM_{2.5}$ > 35 μg $m^{-3}$) are highlighted by the shaded areas.**

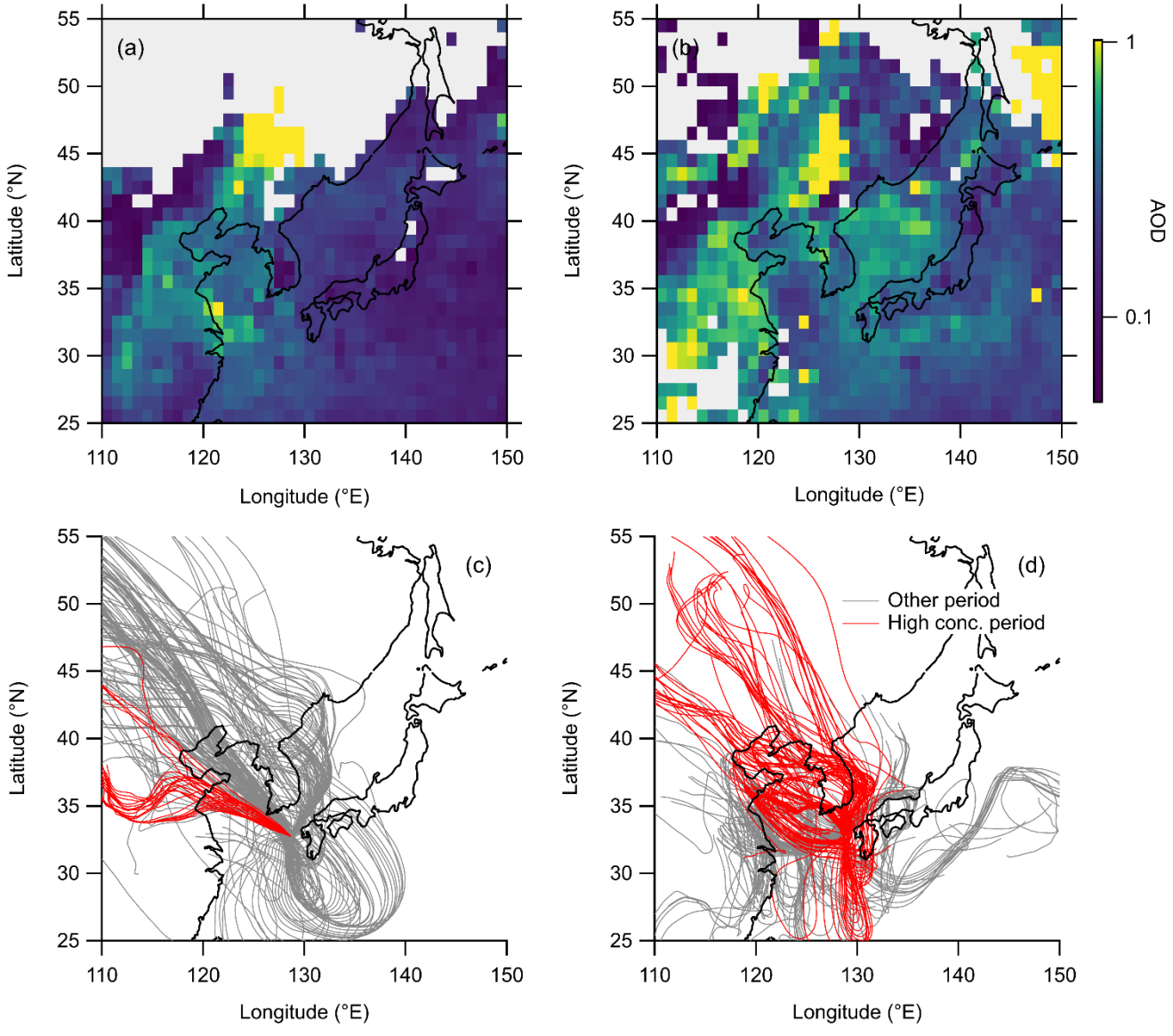


**Figure 2. MODIS-derived AOD spatial distributions for the periods: (a) February 10–17, 2024, and (b) April 15–22, 2024. The backward trajectories for the periods (c) February 10–17, 2024, and (d) April 15–22, 2024. The red colored trajectories were for the high-concentration periods (daily $PM_{2.5}$ > 35 μg $m^{-3}$), as indicated in Fig. 1.**

https://doi.org/10.5194/egusphere-2026-3778
Preprint. Discussion started: 8 July 2026


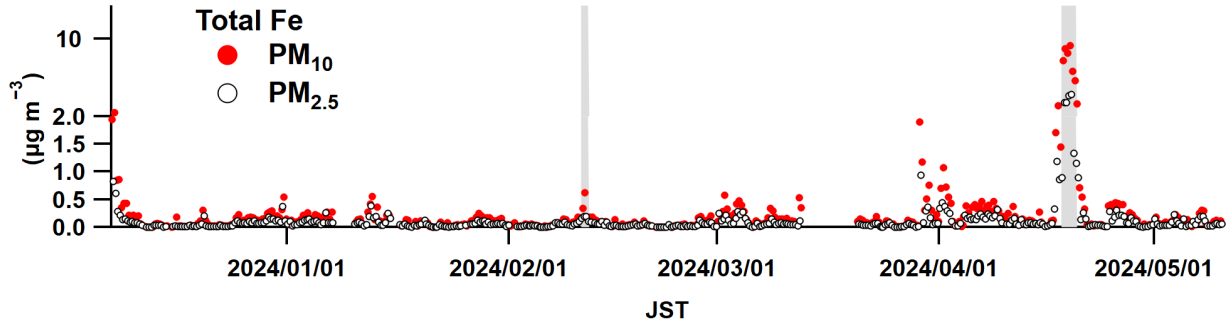


**Figure 3. Temporal variations in the concentrations of $PM_{10}$ (red circles) and $PM_{2.5}$ (open circles) Fe. The selected periods when the Japanese short-term air quality standard for $PM_{2.5}$ was exceeded (daily $PM_{2.5}$ >35 μg $m^{-3}$) are highlighted by shaded areas.**

### 3.3 Source apportionment analyses for $PM_{2.5}$ and $PM_{10}$ aerosols

#### 3.3.1 Validation of multiple linear regression analysis for source apportionment

The source apportionment of $PM_{2.5}$ and $PM_{10}$ aerosols was conducted using the observed BC, Si, and sulfate concentrations ($[BC]_t$, $[Si]_t$, and $[SO_4^{2-}]_t$, respectively). We assumed that the temporal variations in BC concentrations could account for those of both anthropogenic aerosols and a part of secondary aerosol concentrations, and that sulfate concentrations could be used to constrain the secondary formation component through aqueous phase reactions inside aerosol particles and cloud droplets, which cannot be represented by temporal variations in BC concentrations (Miyakawa et al., 2023). The validity of selecting Si, BC, and $SO_4^{2-}$ as input variables for the multiple linear regression (MLR) models was described by Miyakawa et al. (2023). It was concluded that both BC and sulfate can be used for MLR analysis of total mass concentrations. The observed temporal variations in $PM_{2.5}$ and $PM_{10}$ aerosol concentrations ($[PM_{2.5}]_t$ and $[PM_{10}]_t$) were fitted to the following MLR model:

$$\log[PM_{2.5}]_t = \log(g_{BCPM2.5}\cdot[BC]_t + g_{SiPM2.5}\cdot[Si_{PM2.5}]_t + g_{sulfatePM2.5}\cdot[SO_4^{2-}{}_{PM25}]_t + C_{PM2.5}) \quad \text{(Eq. 1)}$$

$$\log[PM_{10}]_t = \log(g_{BCPM10}\cdot[BC]_t + g_{SiPM10}\cdot[Si_{PM10}]_t + g_{sulfatePM10}\cdot[SO_4^{2-}{}_{PM10}]_t + C_{PM10}) \quad \text{(Eq. 2)}$$

The logarithm of the concentrations was analyzed because the variations in the concentrations were very large, resulting in bias when the data were analyzed on a linear scale. The coefficients $g_{XY}$ (X = BC, Si, and sulfate; Y = $PM_{2.5}$ and $PM_{10}$) and $C_Y$ (i.e., constant term for $PM_{2.5}$ or $PM_{10}$ aerosols) were determined using the least squares method. The coefficients of determination of the correlation ($r^2$) between the reconstructed and observed $PM_{2.5}$ and $PM_{10}$ concentrations were 0.92 and 0.94, respectively (**Fig. S9**), and the linear combination model accounted for most of the observed variance in $PM_{2.5}$ and $PM_{10}$ concentrations. $C_Y$ were evaluated to be 2.34 (±0.30) and 3.75 (±0.48) μg $m^{-3}$, which correspond to the background levels of $PM_{2.5}$ and $PM_{10}$ concentrations (including sea-salt aerosols) in the East Asian outflow in the winter–spring of 2023–2024. An

https://doi.org/10.5194/egusphere-2026-3778
Preprint. Discussion started: 8 July 2026


independent method, co-located lidar measurements at the same site, was used to validate our source apportionment results for the dust contribution. Example time series of lidar- and in situ measurement-based extinction coefficients/concentrations for dust and non-dust aerosols are shown in **Fig. 4**.

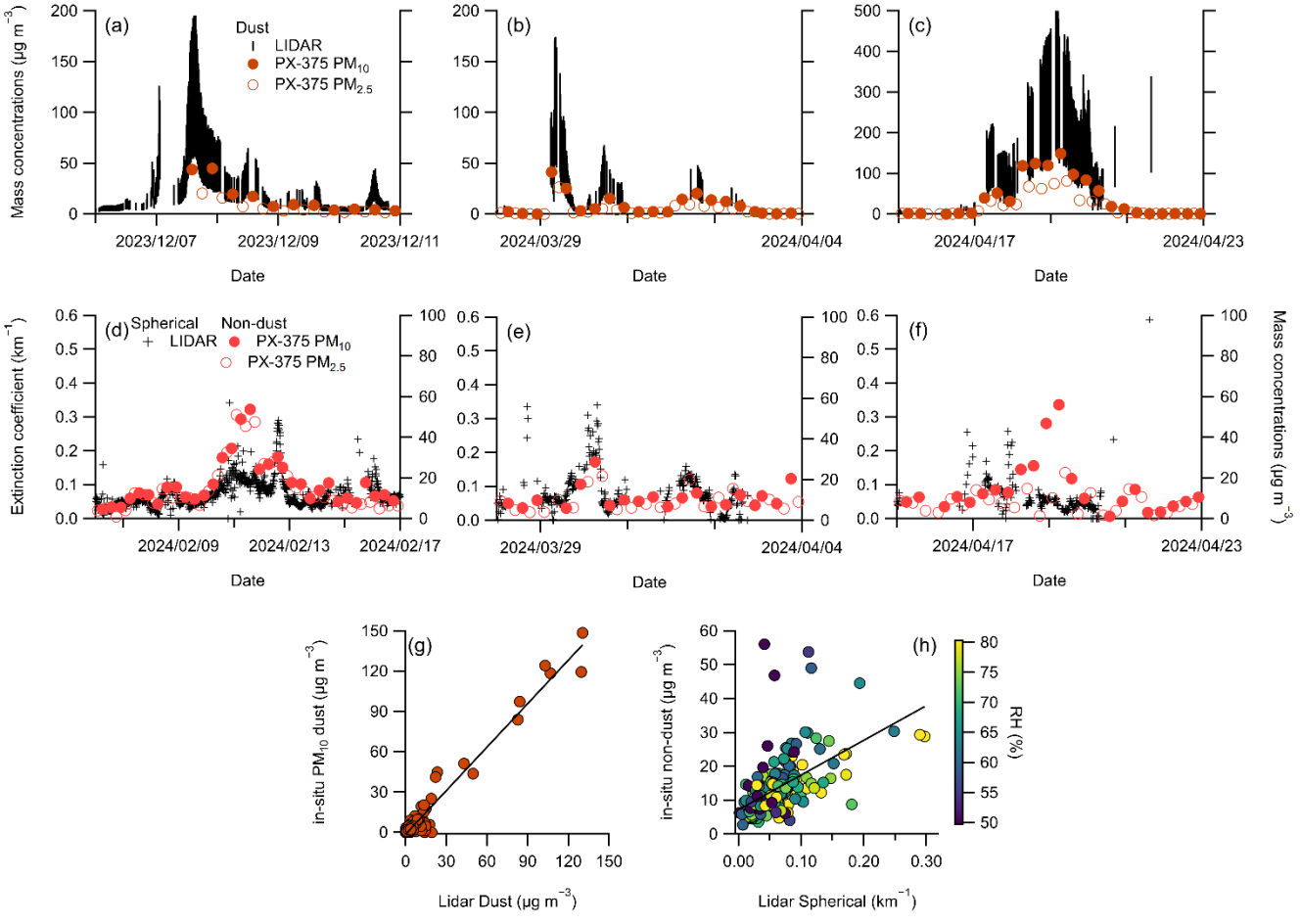


**Figure 4. (a, b, and c) Temporal variations in PX-375-derived (brown open and filled circles for $PM_{2.5}$ and $PM_{10}$ aerosols, respectively) and lidar-derived (black bars) dust mass concentrations for the selected periods. (d, e, and f) Temporal variations in PX-375-derived non-dust mass concentrations (red open and filled circles for $PM_{2.5}$ and $PM_{10}$ aerosols, respectively) and lidar-derived extinction coefficient (black crosses) for the selected periods. The bars in Figs.4a, 4b, and 4c were derived from the assumption of a mass-to-extinction conversion factor σ of 0.5–2 g $m^{-2}$ (Shimizu et al., 2011). (g) Correlation between PX-375-derived $PM_{10}$ dust and lidar-derived dust concentrations with an assumed σ of 0.5 g $m^{-2}$. (h) Correlation between PX-375-derived $PM_{10}$ non-dust concentrations and lidar-derived extinction coefficients. The data points at 4h are colored by $RH_t$ derived from GDAS.**

https://doi.org/10.5194/egusphere-2026-3778
Preprint. Discussion started: 8 July 2026


Lidar-derived dust extinction coefficients were converted to dust mass concentrations by assuming a mass extinction conversion factor of dust aerosols of 0.5–2 g $m^{-2}$ (Shimizu et al., 2011). Lidar-derived dust mass concentrations near the surface were well correlated ($r^2 = 0.95$) with the estimated $PM_{10}$ dust (i.e., $g_{SiPM10} \cdot [Si_{PM10}]_t$) aerosol concentrations during the observation period. Near-surface lidar-derived spherical aerosol extinction coefficients were positively but poorly ($r^2 = 0.28$) correlated with estimated $PM_{10}$ non-dust (i.e., total − dust) aerosol concentrations during the observation periods. The scattered feature of this correlation can be accounted for by the effects of hygroscopic growth on the extinction coefficient measurements using lidar, as indicated by the changes in the ratio with the values of $RH_t$ (**Fig. 4**). These comparisons indicate that this approach can successfully provide the source apportionment of PM, especially dust and non-dust contributions, using high-temporal resolution variations of tracer compounds.

### 3.3.2 Source apportionment of Fe

The estimation of dust contribution using Si as a tracer was validated in Section 3.3.1, and the same approach was applied to the observation-based source apportionment of Fe following Miyakawa et al. (2023). The Eqs. (1) and (2) for the source apportionment of $PM_{2.5}$ and $PM_{10}$ aerosols were modified as Eqs. (3) and (4), respectively.

$$\log[Fe_{PM2.5}]_t = \log(g_{BC,FePM2.5} \cdot [BC]_t + g_{Si,FePM2.5} \cdot [Si_{PM2.5}]_t + C_{FePM2.5}) \quad \text{(Eq. 3)}$$

$$\log[Fe_{PM10}]_t = \log(g_{BC,FePM10} \cdot [BC]_t + g_{Si,FePM10} \cdot [Si_{PM10}]_t + C_{FePM10}) \quad \text{(Eq. 4)}$$

$g_{X,Fe}$ (X = BC and Si) and $C_{Fe}$ (constant term) were determined using the least-squares method. Notably, the BC-related Fe components can be regarded as anthropogenic contributions because Fe does not undergo secondary formation. $C_{Fe}$ for $PM_{2.5}$ and $PM_{10}$ aerosols were almost zero in this study. The $r^2$ between the reconstructed and observed $PM_{2.5}$ and $PM_{10}$ Fe concentrations were 0.99 and 0.98, respectively **(Fig. S9)**, and this linear combination model also accounted for almost all observed variances in $PM_{2.5}$ and $PM_{10}$ Fe concentrations.

The dust contributions to total Fe in $PM_{2.5}$ and $PM_{10}$ aerosols were, on average, 60 % (±25 %) and 72 % (±25 %), respectively. Kurisu et al. (2021; 2026) estimated the anthropogenic and dust Fe concentrations based on the characterization of $\delta^{56}$Fe over the remote ocean in the East Asian outflow and at the same site in 2019–2020, which were used to evaluate the results of this study. The derived ranges were comparable to those estimated using the stable isotope ratio of Fe ($\delta^{56}$Fe) of total ($PM_{2.5}$ + coarse mode) aerosols (60–90 %) in 2019–2020 (Kurisu et al., 2026) and $PM_{2.5}$ (50–90 %) and total aerosols (78–98 %) transported from the East Asian continent to the northwestern Pacific Ocean (Kurisu et al., 2021). The dust contributions to Fe showed seasonal variations, increasing from winter to spring (**Fig. 5**), which can be attributed to the seasonal variations in dust emissions over the source region (e.g., Kurosaki et al., 2005). Kurisu et al. (2026) also indicated a similar seasonal progression of dust contributions in 2019–2020. The Fe content of dust aerosols (CFe) is defined as the concentration of Fe in dust aerosol particles and can be estimated by combining Eqs. 1–4 as follows:

https://doi.org/10.5194/egusphere-2026-3778
Preprint. Discussion started: 8 July 2026


$$CFe_{PM2.5} = g_{Si,FePM2.5} \cdot [Si_{PM2.5}]_t / g_{SiPM2.5} \cdot [Si_{PM2.5}]_t \times 100 = g_{Si,FePM2.5} / g_{SiPM2.5} \times 100 \quad \text{(Eq. 5)}$$

$$CFe_{PM10} = g_{Si,FePM10} \cdot [Si_{PM10}]_t / g_{SiPM2.5} \cdot [Si_{PM10}]_t \times 100 = g_{Si,FePM10} / g_{SiPM10} \times 100 \quad \text{(Eq. 6)}$$

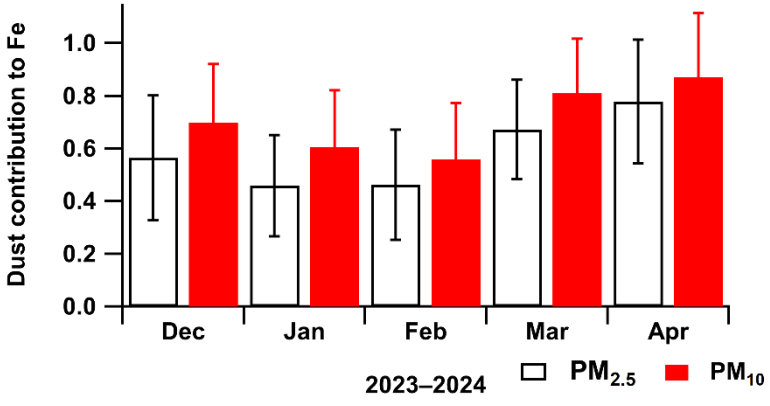


**Figure 5. Monthly mean dust contribution to total Fe for $PM_{2.5}$ (open bars) and $PM_{10}$ (red bars) aerosols from December 2023 to April 2024. Error bars represent standard deviation.**

The CFe values for $PM_{2.5}$ and $PM_{10}$ dust aerosol particles were 4.23 % and 4.87 %, respectively, which are comparable to those (3.98–5.27 %) from previous observational studies (Jeong, 2020; Wang et al., 2011). $g_{BC,FePM2.5}$ and $g_{BC,FePM10}$ represent the enhancement ratios of anthropogenic Fe to BC for $PM_{2.5}$ and $PM_{10}$ aerosols, respectively, and were determined to be 0.11 (±0.02) and 0.15 (±0.03) μg μg$^{-1}$, respectively. Miyakawa et al. (2023) showed a similar value of $g_{BC,FePM2.5}$, 0.13 (±0.03) μg μg$^{-1}$, evaluated at the same site in 2018 using nearly almost the same method. Using the data provided by Kurisu et al. (2026) and BC concentrations at the same site in 2019–2020, the $\delta^{56}$Fe-based enhancement ratios of anthropogenic-Fe to BC for $PM_{2.5}$ and total ($PM_{2.5}$ + coarse) aerosols were evaluated to be 0.08 (±0.03) and 0.17 (±0.08) μg μg$^{-1}$, respectively. Because enhancement ratios of anthropogenic-Fe to BC showed little variation among years and methods, the evaluated enhancement ratios can be considered reliable estimates of anthropogenic-Fe to BC emission ratios over continental regions in East Asia. A potential uncertainty in this analysis is the assumption that the fitted coefficients remained stable during the observation period (i.e., use fixed values), which will be discussed in Section 3.5. The derived results, seasonal variations in dust contributions, Fe content of dust aerosols, and anthropogenic Fe-to-BC ratios, suggest the validity of the source apportionment of Fe in $PM_{2.5}$ and $PM_{10}$ aerosols using high-temporal resolution datasets.

https://doi.org/10.5194/egusphere-2026-3778
Preprint. Discussion started: 8 July 2026


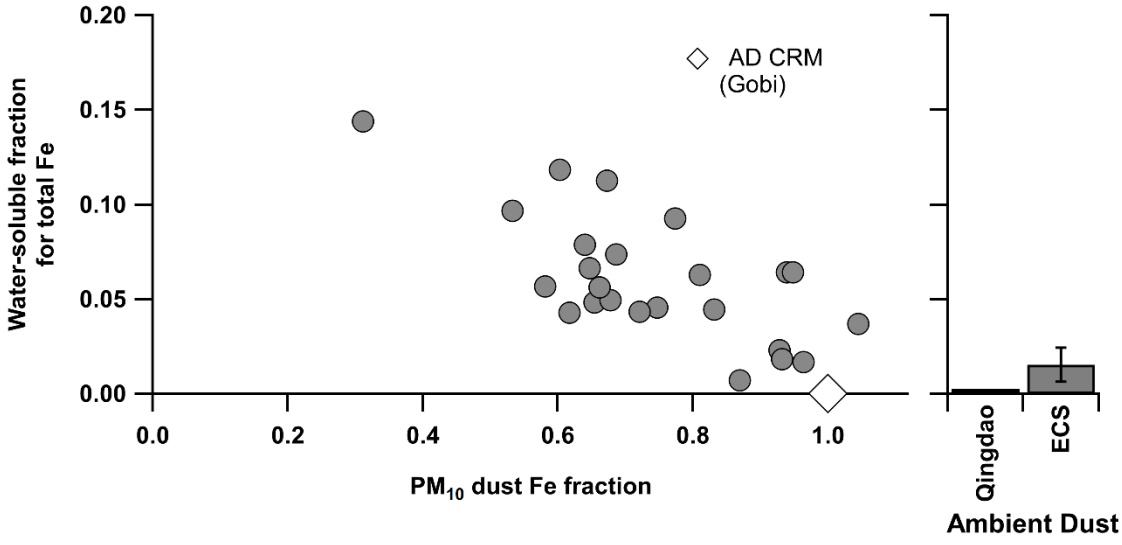


**Figure 6. Relationship between the water-soluble fraction of Fe ($f_{Fe,sol}$) in total aerosols and the dust contribution to total Fe ($R_{dustFe}$) in $PM_{10}$ aerosols (shaded circles). The value of $f_{Fe,sol}$ for the certified reference material of Gobi Desert dust provided by the National Institute for Environmental Studies, Japan (NIES CRM No. 30) is also shown as an open diamond in the left panel. The $f_{Fe,sol}$ values for ambient dust aerosols in Qingdao, China (Shi et al., 2020) and over the East China Sea (Hsu et al., 2010) are shown in the right panel.**

### 3.4 Variations in the fractional contributions and concentrations of water-soluble Fe

The fractional solubility of Fe ($f_{Fe,sol}$) was analyzed as a proxy of bioaccessibility of Fe in terms of the factors considered to affect their variability, as described in Section 1. The contributions of dust to Fe ($R_{dustFe}$) for $PM_{2.5}$ and $PM_{10}$ aerosol particles were evaluated using the MLR analyses of Fe (see section 3.3.2). The $R_{dustFe}$ for coarse mode particles was estimated based on the differences in $R_{dustFe}$ between $PM_{2.5}$ and $PM_{10}$ aerosol particles. The $R_{dustFe}$ values were compared with $f_{Fe,sol}$ for total, fine-, and coarse-mode particles (**Figs. 6 and 7a–b**). The variability in $f_{Fe,sol}$ for total and fine-mode aerosol particles was negatively correlated with that in $R_{dustFe}$. The $f_{Fe,sol}$ of the certified reference material for Gobi Desert dust (NIES CRM No. 30), 0.02 % (i.e., the diamond marker at $R_{dustFe} = 1$ in **Fig. 6**) corresponds well with the lower end of the anticorrelation relationship between $f_{Fe,sol}$ and $R_{dustFe}$. The $f_{Fe,sol}$ of ambient aerosols for total suspended particulate (TSP) matter during dust events (i.e., the higher $R_{dustFe}$ period) were evaluated in Qingdao, China (Shi et al., 2020) and over the East China Sea (Hsu et al., 2010) to be 0.27 % and 1.54 %, respectively (**Fig. 6**), which were comparable to our observations with $R_{dustFe}$ of approximately 1. The observed feature of the strong dependence of $R_{dustFe}$ on $f_{Fe,sol}$ indicates the importance of the source apportionment of Fe. As the variability in $f_{Fe,sol}$ for fine-mode particles was much higher than that for coarse-mode particles, $f_{Fe,sol}$ for total aerosol particles was weakly but significantly regulated ($r^2 = 0.47$, $p < 0.01$) by the ratios of $PM_{2.5}$ to $PM_{10}$ mass ratio for Fe (**Fig. S10**). We suggest that the characterizations of Fe with multiple size cuts using an online or semicontinuous instrument (e.g., PX-375) are also beneficial for estimating the variabilities in $f_{Fe,sol}$ for total aerosol particles with a high temporal resolution (e.g., < 1

https://doi.org/10.5194/egusphere-2026-3778
Preprint. Discussion started: 8 July 2026


d) without chemical analyses of $Fe_{sol}$. Variabilities in $f_{Fe,sol}$ for fine-mode particles were also affected by those in $R_{dustFe}$ (**Fig. 7a**); however, their correlations were scattered compared to total aerosol particles. 2-end members of $f_{Fe,sol}$ for fine-mode anthropogenic and dust particles were estimated based on $\delta^{56}$Fe characterizations at the same site in 2019–2020 (Kurisu et al., 2026), and their mixing partly accounts for the variabilities in $f_{Fe,sol}$ for fine-mode anthropogenic measured in this study.

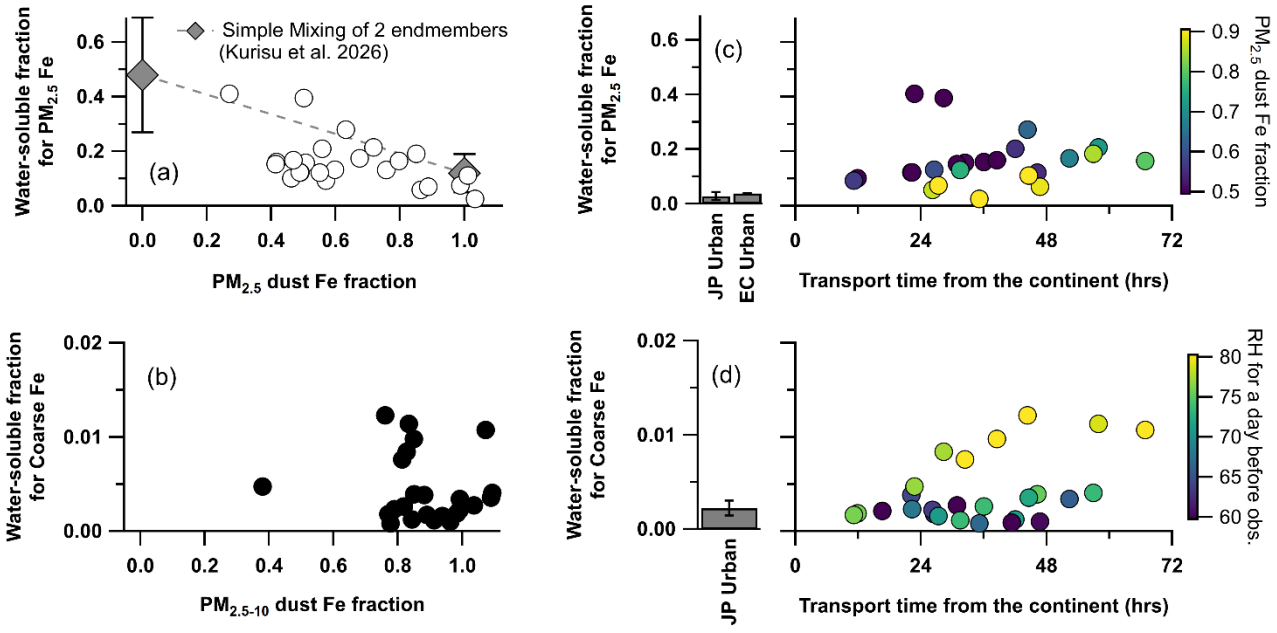


**Figure 7. (a) Relationship between the water-soluble fraction of Fe ($f_{Fe,sol}$) in $PM_{2.5}$ aerosols and dust contribution to total Fe ($R_{dustFe}$) in $PM_{2.5}$ aerosols (open circles). The $f_{Fe,sol}$ of 2-end members for anthropogenic and dust aerosols evaluated by Kurisu et al. (2026) are shown in Fig.7a. (b) Relationship between $f_{Fe,sol}$ for coarse aerosols and $R_{dustFe}$ for coarse aerosols ($PM_{10}$-$PM_{2.5}$) (black circles). Changes in $f_{Fe,sol}$ for (c) $PM_{2.5}$ and (d) coarse aerosols as a function of transport time from the continent. As a reference for $f_{Fe,sol}$ near emission sources (transport time close to zero), $f_{Fe,sol}$ in Yokosuka (this study) and Eastern Chinese urban cities (Zhu et al., 2020) for $PM_{2.5}$ and coarse (only for Yokosuka) aerosols are shown in Figs.7c and 7d, respectively. The data points in Fig. 7c are colored by $R_{dustFe}$ for the $PM_{2.5}$ aerosols. The data points at Fig. 7d are colored by the RH averaged for a day before the observations ($RH_{-1d}$).**

**Figures 7c** and **d** depict the relationship between $f_{Fe,sol}$ for fine- and coarse-mode particles and the transport time from the continent, estimated using backward trajectories. These relationships suggest that air mass aging can affect the variability in $f_{Fe,sol}$, especially for coarse-mode particles. At least, $f_{Fe,sol}$ in both mode particles were systematically higher in more aged air masses (e.g., >2 d) than in less-aged air masses (e.g., <~1 d). The values of $f_{Fe,sol}$ near the source regions were compared. The $f_{Fe,sol}$ values for fine- ($PM_{2.5}$) and coarse-mode particles were 2.8 % and 0.2 %, respectively, at the Yokosuka site, Japan, in the fall of 2022. Zhu et al. (2020) evaluated $f_{Fe,sol}$ for $PM_{2.5}$ aerosols to be 2.7–5.0 % at 4 urban sites (Beijing, Handan, Hangzhou, and Zhengzhou) in East China in the winter of 2017. Combining these with the results at the Fukue site, we found that $f_{Fe,sol}$ rapidly increased within a day, especially for fine-mode particles. The increasing tendency of $f_{Fe,sol}$ during transport was source-

https://doi.org/10.5194/egusphere-2026-3778
Preprint. Discussion started: 8 July 2026


dependent, as shown in **Figs. 7c and 7d**. $f_{Fe,sol}$ in dust-dominated air masses (e.g., yellowish markers in **Fig. 7c**) showed slower increases than in other air masses with dust contributions below ~60 %, indicating that the rate of increase in $f_{Fe,sol}$ can be source-specific. Some data points in **Fig. 7d** show higher $f_{Fe,\ sol}$ values in moderately aged air masses (1–2 d). These data have different air mass histories. The average relative humidity for a day before the observations ($RH_{-1d}$) and accumulated precipitation along trajectories (APT) for 3 days before the observations were calculated using backward trajectories with GDAS data and were compared with $f_{Fe,sol}$ (**Figs. 8a–b**). When $RH_{-1d}$ exceeded 75–80 %, $f_{Fe,sol}$ for the coarse-mode particles significantly increased (**Fig. 8b**).

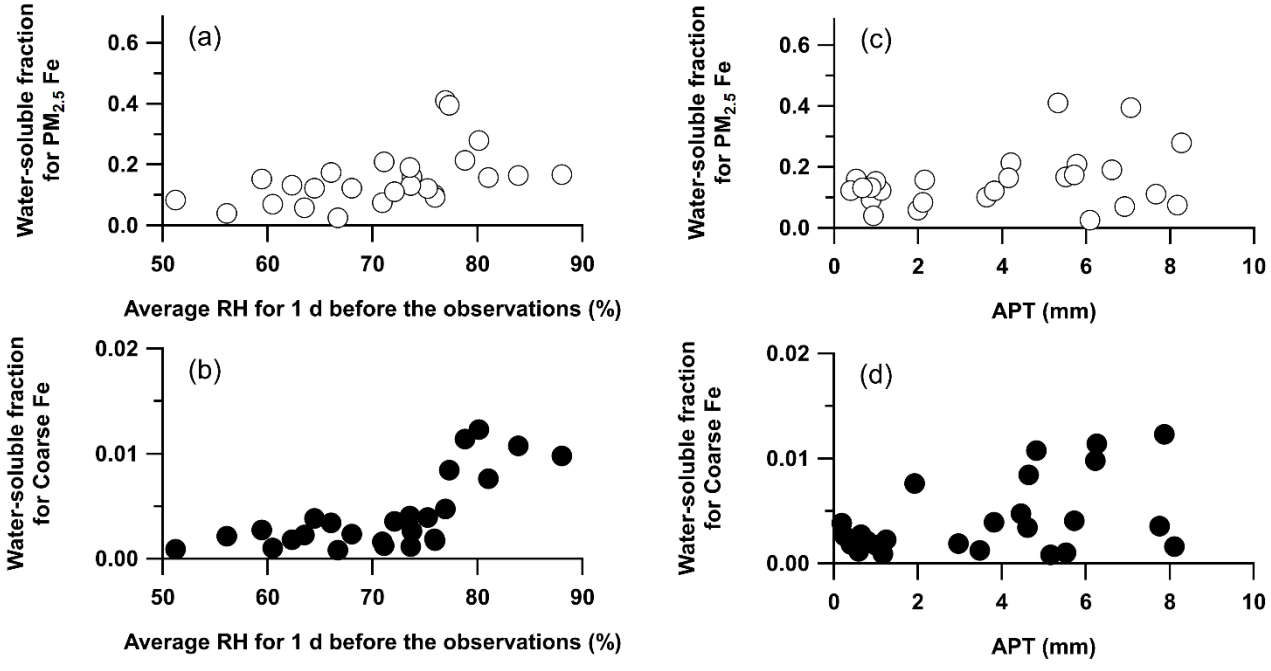


**Figure 8. (a) Relationship between water-soluble fraction to Fe ($f_{Fe,sol}$) for $PM_{2.5}$ aerosols and RH averaged for a day before the observations ($RH_{-d}$) (open circles). (b) Relationship between $f_{Fe,sol}$ for coarse aerosols and $RH_{-1d}$ (black circles). (c) Relationship between $f_{Fe,sol}$ for $PM_{2.5}$ aerosols and accumulated precipitation along trajectories (APT) (open circles). (d) Relationship between $f_{Fe,sol}$ for coarse aerosols and APT (black circles).**

As the $PM_{10}$ sulfate-to-dust or BC concentration ratios increased with $RH_{-1d}$ (**Fig. S11**), the aqueous-phase production of acidic species under high $RH_{-1d}$ conditions likely affected the increase in $f_{Fe,sol}$. This can be observational evidence that aqueous-phase processing affects the variability in $f_{Fe,sol}$ for mineral dust particles (e.g., Sakata et al., 2025; Shi et al., 2015). APT was used as an indicator of the wet removal of BC (Kanaya et al., 2016) and trace metals (Miyakawa et al., 2023) during transport. If the preferential removal of $Fe_{sol}$ by cloud processing (including precipitation) dominates, $f_{Fe,sol}$ would decrease with an increase in APT. **Figures 8c and 8d** showed no decreasing trend of $f_{Fe,sol}$ against the APT and suggest no such preference in the wet removal of Fe. Because particle size as well as water solubility are important in the CCN formation process under

https://doi.org/10.5194/egusphere-2026-3778
Preprint. Discussion started: 8 July 2026


moderate supersaturation conditions (e.g., Dusek et al., 2006), aerosols containing both water-soluble and insoluble Fe were likely removed during wet removal processes during transport. The relationships obtained between $f_{Fe,sol}$ and air mass histories can be useful constraints for evaluating and refining model simulations of the processes controlling $f_{Fe,sol}$.

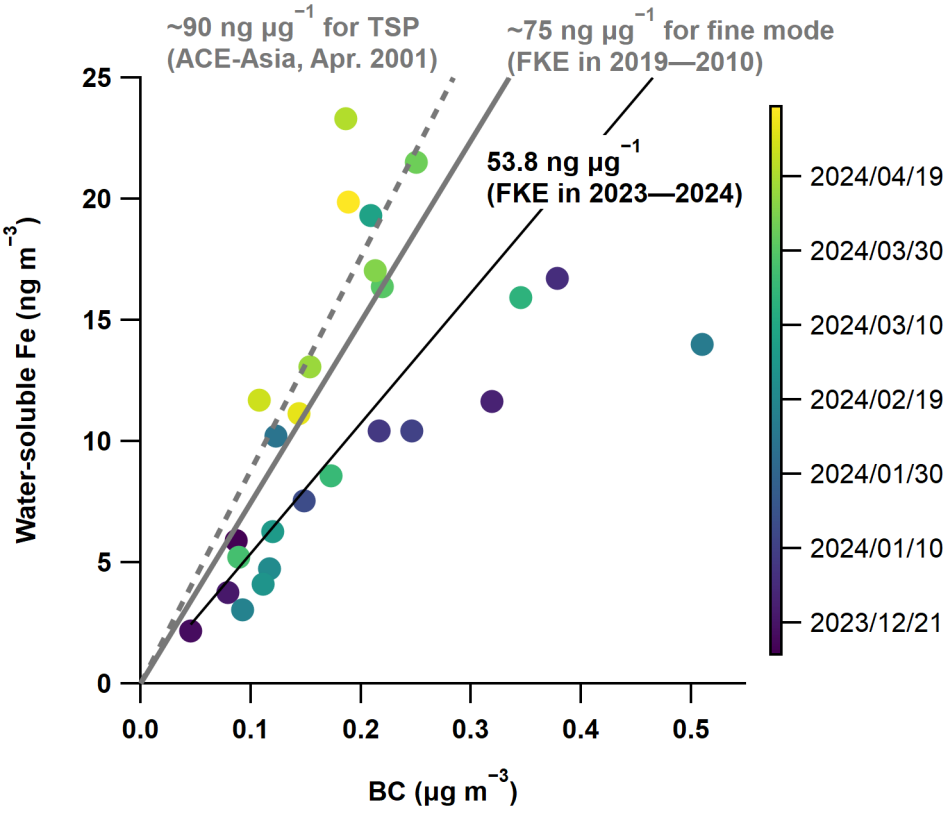


**Figure 9. Correlation of water-soluble Fe ($Fe_{sol}$) concentrations in total (fine + coarse) aerosols with BC concentrations. The data points are colored according to the date and time (JST) of the observation period. The black solid line depicts the fitted line for this correlation. The solid and dashed gray lines depict the slopes of the correlations between $Fe_{sol}$ and BC (EC) as reported by Kurisu et al. (2026) and Chuang et al. (2005), respectively.**

We found that temporal variations in total water-soluble Fe ($Fe_{sol}$) concentrations derived from HVS were closely related to those of BC concentrations (**Fig. 9**). Most of the $Fe_{sol}$ masses were in fine-mode particles, which is consistent with the good correlation ($r^2$ = 0.93) between $Fe_{sol}$ and BC. The enhancement ratio of $Fe_{sol}$ to BC ($\Delta Fe_{sol}/\Delta BC$) was 53.8 (±11) ng $\mu g^{-1}$ on average, and it seasonally increased from winter (~40 ng $\mu g^{-1}$) to spring (~90 ng $\mu g^{-1}$). As the dust contribution to Fe in $PM_{2.5}$ and $PM_{10}$ aerosols slightly increased from winter to spring, $f_{Fe,sol}$ for the "bulk" total aerosols slightly decreased from winter to spring in 2023–2024. However, the dust Fe concentrations increased from winter to spring during the observation period and were much higher than the anthropogenic Fe in spring, indicating the significant contributions of dust to $Fe_{sol}$ in spring, regardless of their low water solubility. Kurisu et al. (2026) analyzed the model-based source attributions of anthropogenic Fe at the same site in the winter–spring of 2019–2020, indicating that the contributions of coal combustion (i.e., energy, industrial,

https://doi.org/10.5194/egusphere-2026-3778
Preprint. Discussion started: 8 July 2026


and residential), steel manufacturing, and traffic emissions were dominated and showed no large seasonal variations of their relative contributions during the studied period. We thus suggest that the observed seasonal changes in $\Delta Fe_{sol}/\Delta BC$ can be partly attributed to the reduction of BC emissions from the residential sector over China in the seasonal transition (Kanaya et al., 2016) because of the dominance of residential sector for BC emissions in China (64 % on average, see Kanaya et al. (2021) for details). The seasonal progress of $\Delta Fe_{sol}/\Delta BC$ was further analyzed using the model simulation in Section 3.5.

### 3.5 Evaluations and analyses of the IMPACT model simulations

The simulation results of BC, Fe, and $Fe_{sol}$ concentrations and the source apportionments of Fe using the IMPACT model were thoroughly evaluated using the observed datasets. All simulated parameters were significantly correlated with those observed/estimated (**Table S4**). The normalized mean bias (NMB) for the simulated BC concentrations was 34.9 %, indicating that the IMPACT model likely overestimated aerosol emissions from anthropogenic combustion sources (**Fig. S12**). The positive NMBs for anthropogenic Fe in $PM_{2.5}$ and $PM_{10}$ aerosols can also be attributed to the overestimation of aerosol emissions from anthropogenic combustion sources (**Fig. S13**). In contrast, the IMPACT model underestimated the dust Fe concentrations, especially during the high-concentration period (April 18–20, 2024) (**Fig. S14**). Overall, the total Fe concentrations were underestimated because of the underestimation of dust Fe concentrations, which overwhelmed the overestimation of anthropogenic Fe concentrations (**Fig. S15**). The model simulations for total Fe aerosols ($PM_{20}$ for the model and $PM_{10}$ for the observations) showed relatively poor correlations ($r^2 = 0.39$) to those for $PM_{2.5}$ Fe aerosols ($r^2 = 0.66$). This can be partly derived from the uncertainties in the dry deposition fluxes of coarse particles in the model (Kok et al., 2021). As the high temporal resolution variations in the source-resolved Fe concentrations were reasonably well simulated, we concluded that the removal processes as well as emissions were also reasonably simulated. Variations in $Fe_{sol}$ concentrations were reasonably well simulated ($r^2 = 0.56$) using the IMPACT model. However, the $Fe_{sol}$ concentrations for $PM_{2.5}$ aerosols were underestimated (NMB of −23.7 %), whereas those for total ($PM_{2.5}$ + coarse) aerosols were overestimated (NMB of 21 %) by the IMPACT model (**Fig. S16**). The underestimation of $Fe_{sol}$ concentrations for $PM_{2.5}$ aerosols can partly be accounted for by the uncertainties of the size cut performance of the impactor used for the HVS ($PM_{2.5}$ Fe characterization was biased by ~30 %, Fig. S4), as described in section 3.1. Therefore, the comparison results of $Fe_{sol}$ concentrations for total aerosols can be analyzed to assess the performance of the IMPACT model with minimized uncertainties in the observations. Ito et al. (2020) indicated that the IMPACT model well reproduced the values of $f_{Fe,sol}$ measured by a leaching method using an ammonium acetate buffer solution, which showed systematically higher values of $f_{Fe,sol}$ than those measured by the leaching method used in this study (i.e., ultrapure water dissolution) (Tang et al., 2025). This difference can be attributed to the pH of the solution (Perron et al. 2020). Therefore, the possible reason for the discrepancies between the observations and model simulations (NMB of 21 %) in this study was the type of leaching method used to derive the $Fe_{sol}$ concentrations. Further characterization of $Fe_{sol}$ concentrations and $f_{Fe,sol}$ using different leaching methods is needed to observationally derive the range of $f_{Fe,sol}$ and to compare them with the model simulations. However, based on these evaluations of the simulation results of the IMPACT model, we

https://doi.org/10.5194/egusphere-2026-3778
Preprint. Discussion started: 8 July 2026


concluded that the model data of $Fe_{sol}$ concentrations and depositions for total aerosols can be further analyzed to draw regional-scale features of Fe in the East Asian outflow regions.

The correlations between the $Fe_{sol}$ and BC concentrations simulated by the IMPACT model are shown in **Fig. 10**. The modeled $\Delta Fe_{sol}/\Delta BC$ for total Fe varied similarly to those observed, showing seasonal changes from winter to spring (**Fig. 10a**). In contrast, the modeled $\Delta Fe_{sol}/\Delta BC$ for anthropogenic Fe was relatively stable compared to that for total Fe, but with small increases from winter to spring during the observation period (**Fig. 10b**). The monthly mean fractional contributions of the residential sector to the $Fe_{sol}$ and BC concentrations at the observation site are shown in **Fig. S17**. The contributions of the residential sector decreased by 23 % for BC and 3 % for anthropogenic $Fe_{sol}$ from December 2023 to April 2024, which can account for the changes in $\Delta Fe_{sol}/\Delta BC$ for anthropogenic Fe, as shown in **Fig. 10b**. Therefore, we concluded that the observed seasonal variations in $\Delta Fe_{sol}/\Delta BC$ can be attributed primarily to changes in the dust contributions to $Fe_{sol}$ and partly to changes in the emission source strength of the residential sector for BC. The predicted small contributions of the residential sector to $Fe_{sol}$ concentrations during the observation period (1–4 %, **Fig. S17**) is smaller than those (~30%) on $Fe_{sol}$ emissions and deposition fluxes in East Asia suggested by Cui et al. (2025) and Li et al. (2026). This may be partly accounted for by the differences in the bioaccessibility of Fe at the emission and aging during transport among model simulations. If our simulations substantially underestimate $Fe_{sol}$ from the residential sector and accurately evaluate the others, the current overestimations of $Fe_{sol}$ concentrations (**Fig. S16**) become worse by adding the underestimated portion of $Fe_{sol}$ from the residential sector. Further observations integrating the detailed source attribution segregating fuel types and/or emission processes, for example stable isotope ratio measurements of $Fe_{sol}$ (Kurisu et al., 2026), are crucially needed for better constraining the model simulations. It should be noted that the predicted reductions in the BC emissions from residential sectors from winter to spring imply the potential uncertainty in assuming the fixed fitting coefficients (e.g., $g_{BC,FePM2.5}$) for the BC component in the MLR model throughout the observation period (section 3.3.2). These coefficients can be higher (lower) than the calculated values in spring (winter), but the difference cannot be large (<~20 %). The modeled $\Delta Fe_{sol}/\Delta BC$ well predicted those observed, even though the modeled concentrations of $Fe_{sol}$ and BC were positively biased (NMB of 21 % and 34.9 %, respectively). This parameter can be useful for diagnosing the model performance in predicting both the source apportionment (anthropogenic vs. natural sources) of $Fe_{sol}$ and its atmospheric processing.

https://doi.org/10.5194/egusphere-2026-3778
Preprint. Discussion started: 8 July 2026


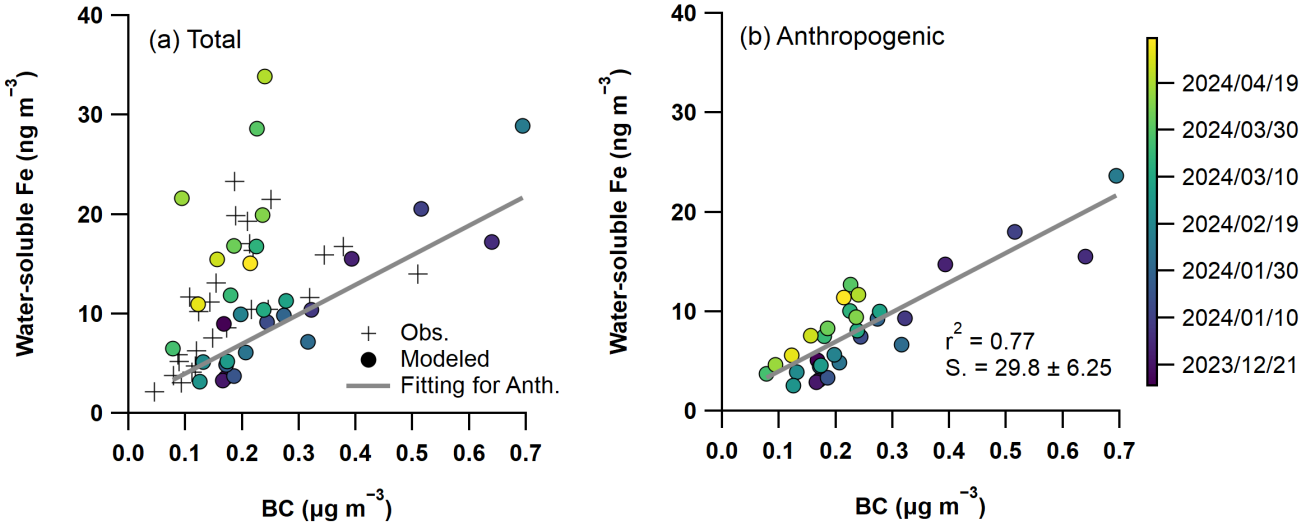


**Figure 10. Correlation of BC and water-soluble Fe ($Fe_{sol}$) concentrations for (a) total (fine + coarse) and (b) anthropogenic Fe simulated using the IMPACT model. The data points in Figs.10a and 10b are colored according to the date and time (JST) during the observation period. The black cross markers in Fig.10a depict the observed correlations between $Fe_{sol}$ and BC (the same data used in Fig. 9). The shaded solid line depicts the fitted line for the correlation between anthropogenic $Fe_{sol}$ and BC.**

The modeled depositions of dust and $Fe_{sol}$ over the NWPO were compared with those investigated by Nagashima et al. (2023) (**Fig. S18**). They analyzed quartz-containing mineral particles suspended in surface seawaters at the oceanic observation site "K2" (47° N, 160° E) during 11 research cruises from 2003 to 2022 and estimated the seasonal variations in the deposition flux of dust and $Fe_{sol}$ over the NWPO by assuming the fixed values of $C_{Fe}$ (5.3 %) and $f_{Fe,sol}$ (1.1 %) for Asian dust. The simulated dust Fe and dust $Fe_{sol}$ deposition flux at the K2 site in 2024 showed similar seasonal variations (spring maxima) and the same orders (~0.1 mg m$^{-2}$ d$^{-1}$ and ~1 μg m$^{-2}$ d$^{-1}$, respectively) as those observed in 2003–2022. The modeled dust contribution to total $Fe_{sol}$ deposition overwhelmed the others (anthropogenic and pyrogenic sources) in spring (March–April). Bioavailable Fe can be supplied from Fe-rich intermediate waters to surface seawater in the NWPO, which significantly affects springtime biological production and biogeochemical cycles in the NWPO (e.g., Nishioka et al., 2007; 2020). In Nagashima et al. (2023), the intermediate water-sourced bioavailable Fe supply at the K2 site in the spring–summer seasons was also estimated to be c.a. 2.0 μg m$^{-2}$ d$^{-1}$, which was comparable to our modeled estimates of the atmospheric water-soluble (bioaccessible) Fe supply. The model simulations implied that the long-range transport of dust Fe from the continent in East Asia and its deposition in the outflow oceanic regions over the NWPO can control the atmospheric supply of bioaccessible Fe to the ocean surface in the HNLC region and contribute to the significant amount of bioavailable Fe required for sustaining the springtime ocean biological activities in the NWPO.

https://doi.org/10.5194/egusphere-2026-3778
Preprint. Discussion started: 8 July 2026


## 4 Implications and future work

### 4.1 Source apportionments and water-soluble fraction of other elements

In this study, we analyzed the datasets of concentrations and water-soluble fractions only for Fe. We successfully obtained high-temporal-resolution concentrations and size-resolved water-soluble fraction of multiple metallic elements other than Fe, such as Ti, V, Cr, Mn, Ni, Cu, Zn, As, and Pb, in $PM_{2.5}$ and $PM_{10}$ aerosols. The leachable fractions of these metallic elements in aerosols are also key parameters for assessing their impacts on ocean microbiology. Mn as well as Fe play a role as growth-limiting nutrients for marine phytoplankton in HNLC regions, such as the NWPO and Southern Ocean (Mahowald et al., 2018, and references therein). Other trace metals can also limit microbial biogeochemistry (e.g., Zn; Moore et al., 2013), and their higher concentrations can be toxic to some plankton (e.g., Cu; Jordi et al., 2012). These indicate that atmospheric deposition of the trace metals onto the ocean surface can alter community composition and potentially inhibit biological productivity. Modeling attempts to simulate the multi-elemental compositions of atmospheric aerosols and their deposition have been challenging. Only a limited number of studies have addressed this issue, especially in East Asia (Chatani et al., 2021; Kajino et al., 2020; 2021; Ito and Miyakawa, 2023). Further characterizations of various trace metals in terms of source apportionments and bioaccsessibility using our datasets are urgently required to derive a comprehensive understanding of the environmental impacts of trace metals in East Asian outflow regions through synergetic work using numerical model simulations.

### 4.2 Considerations in the methods to analyze water-soluble fraction of Fe

Ultrapure water was used to extract the $Fe_{sol}$ content from the aerosols collected on the filters in this study. This method was based on that of Buck et al. (2013). As described in Section 2.3, the value of $f_{Fe,sol}$ using ultrapure water is recognized as a lower estimate. Tang et al. (2025) compiled the results from an inter-laboratory intercomparison study for trace metal leaching methods that analyzed ambient aerosol samples and clarified the lower estimate of $f_{Fe,sol}$ based on ultrapure water leaching by comparing the methods using acetic acid (Berger et al., 2008) and ammonium acetate (Peron et al., 2020) solutions. Previous studies have suggested that $f_{Fe,sol}$ measured using ultrapure water leaching is comparable to or higher than that measured using seawater leaching (Buck et al., 2010; Shelley et al., 2018). As the dissolution of Fe into the water phase can be dependent on the composition of the solution, for example, organic ligand concentrations (e.g., Paris and Desboeufs, 2013), it is difficult to experimentally mimic seawater dissolution of Fe, which can be applicable to a wide range of oceanic conditions. To derive the possible range of $f_{Fe,sol}$ and harmonize the $f_{Fe,sol}$ datasets with those obtained in different studies, further studies integrating multiple Fe leaching methods are needed in East Asian outflow regions.

https://doi.org/10.5194/egusphere-2026-3778
Preprint. Discussion started: 8 July 2026


### 4.3 Insights into long-term variations in $Fe_{sol}$ concentrations in the East Asian outflow regions

Kurisu et al. (2026) analyzed $f_{Fe,sol}$ for fine-mode particles at the same site in the winter and spring of 2019–2020. Using our BC datasets, the $\Delta Fe_{sol}/\Delta BC$ in 2019–2020 was evaluated to be 74.7 (±21) ng $\mu g^{-1}$ on average. Chuang et al. (2005) found a similar relationship between $Fe_{sol}$ in TSP and EC concentrations at the Gosan supersite on Jeju Island, Korea, during the Aerosol Characterization Experiment–Asia campaign (March 31–May 2, 2001). The enhancement ratio of $Fe_{sol}$ to EC ($\Delta Fe_{sol}/\Delta EC$) was ~90 ng $\mu g^{-1}$. Although the measurement techniques of BC (i.e., light absorption method) and EC (i.e., thermal-optical method, Schauer et al., 2003) differed among studies, springtime $\Delta Fe_{sol}/\Delta EC$ in 2001 was comparable to $\Delta Fe_{sol}/\Delta BC$ in 2023–2024 (**Fig. 9**). Careful data harmonization for both BC and $Fe_{sol}$ is needed for a more precise comparison with previous studies. The observed relationship between $Fe_{sol}$ and BC concentrations reported in this study provides useful constraints for evaluating model predictions of $Fe_{sol}$ in the East Asian outflow regions. The recent significant decreasing trend of BC near the source region over the continent (e.g., Xie et al., 2025) and in East Asian outflow (e.g., Kanaya et al., 2020) suggests that $Fe_{sol}$ concentrations in East Asia may have decreased since 2010–2020s. A climate-change-related decrease in mineral dust emissions over the continental region has also been indicated (Wu et al., 2022). Satellite-based observations suggest that recent climate change (2003–2021) has significantly affected air-pollution transport from continental sources to outflow regions in winter–spring (Cai et al., 2024). The reduced delivery of $Fe_{sol}$ to the HNLC region, as predicted by a modeling study (Zhu et al., 2025), may have modulated the impacts of atmospheric bioaccessible Fe supply in this region. Long-term simulations using the IMPACT model will be essential for investigating long-term trends and interannual variations in $Fe_{sol}$ concentrations in the East Asian outflow and their deposition onto the HNLC region over the NWPO in terms of their relative importance compared with those from intermediate waters.

### 4.4 Perspectives to further evaluate model simulations of airborne concentrations of bioaccessible Fe in aerosols and their deposition to the ocean surface

As the observation site is located in a gateway region for continental air-mass transport to the NWPO under the East Asian winter monsoon system, our datasets—affected by multiple sources and aging processes during transport—provide useful constraints for simulating not only source-resolved Fe concentrations but also complex interactions between Asian dust and atmospheric pollution. Further elaborate studies involving model simulations with our datasets are critically needed to investigate the transport and supply of bioaccessible Fe to the NWPO. To this end, the observational results of this study need to be compared with global atmospheric models that can simulate atmospheric concentrations, source apportionments, and the fractional solubility of Fe in aerosol particles. Our datasets were characterized by high temporal resolution Fe and tracer concentrations and source apportionment with different size cuts (i.e., $PM_{2.5}$ and $PM_{10}$) and mode-segregated $f_{Fe,sol}$. The former is beneficial for evaluating the transport processes as well as source-resolved emission strengths of Fe in East Asian regions. Indeed, Miyakawa et al. (2023) analyzed high temporal resolution data of the concentrations of Fe and other tracer compounds (e.g., BC) with the IMPACT model simulations (Ito and Miyakawa, 2023) and pointed out the overestimation of anthropogenic

https://doi.org/10.5194/egusphere-2026-3778
Preprint. Discussion started: 8 July 2026


Fe emission strength and uncertainties in the wet removal processes of elements related to anthropogenic emissions (e.g., Cu and Pb) in the IMPACT model. The latter is unequivocally required to quantitatively assess the role of Fe in ocean biogeochemistry. Model evaluations with our datasets will provide an opportunity to improve the simulated supply of bioaccesible Fe to the oceans in the East Asian outflow region, such as the NWPO. In this study, we compared observed Fe and $Fe_{sol}$ concentrations and Fe source apportionment results, with simulations from the updated IMPACT model. The current version of the IMPACT model reasonably simulated $Fe_{sol}$ concentrations at the observation site; however, it overestimated (underestimated) the anthropogenic (dust) Fe concentrations, resulting in overestimations of $f_{Fe,sol}$. To further validate the IMPACT model, multi-model approaches involving other models participating in intercomparison studies under discussion in the GESAMP Working Group 38 (e.g., Johnson and Meskhidze, 2013; Myriokefalitakis et al., 2015; Scanza et al., 2018) are of great interest for assessing the schemes adapted in the models to describe the aging processes of Fe during transport and the performance of simulating transboundary transport of Asian dust aerosols to the NWPO. Other HNLC regions in the southern hemisphere (SH), such as the Southern Ocean, should also be targeted because bioaccessible Fe sources in the HNLC regions remain poorly understood. The observation setups used in this study, which combined high-temporal resolution multielement (especially Si as well as Fe) and tracer (e.g., BC) concentrations and $f_{Fe,sol}$ for size-segregated aerosols, would be useful for investigating the roles of mineral dust from desert regions and combustion aerosols from biomass burning in the supply of bioaccessible Fe to the ocean in the SH (e.g., Cosentino et al., 2020; Desboeufs et al., 2024; Ito et al., 2017; 2020).

## 5 Conclusions

Trace metals in aerosol particles impact Earth's radiative budget, human health, and ocean biogeochemistry. Semi-continuous measurements of the elemental composition of fine-mode ($PM_{2.5}$) and total ($PM_{10}$) aerosols and high-volume air sampling (5-d)/offline chemical analyses were conducted on a remote island of Japan in the winter–spring of 2023–2024 to characterize the source apportionment and water-soluble concentrations and fractions of geochemically important elements such as Fe in the East Asian outflow region. $PM_{2.5}$ ($PM_{10}$) total aerosol and Fe concentrations reached 85 (205) and 2.7 (7.4) μg $m^{-3}$, respectively (April 18–20, 2024). Backward trajectories and satellite observations during this period indicated a strong influence of Asian dust transport on the outflow region. The values of $f_{Fe,sol}$ greatly varied from 3 % to 40 % for $PM_{2.5}$ aerosols and were less than 1.5 % for coarse mode aerosols (>2.5 μm), indicating that mineral dust dominated the coarse mode and that $R_{dustFe}$ temporally varied for $PM_{2.5}$ aerosols. Temporal variations in $PM_{2.5}$ and $PM_{10}$ Fe concentrations were analyzed based on MLR using the concentrations of tracer species (Si and BC) and were classified into dust and non-dust Fe contributions for $PM_{2.5}$ and coarse-mode aerosols. Size-segregated $f_{Fe,sol}$ was investigated using $R_{dustFe}$ and aging processes (transport time, RH, and increases in sulfate mass). The source apportionment (dust vs. non-dust) was essential to account for the $f_{Fe,sol}$ variations for $PM_{2.5}$ aerosols, whereas coarse mode aerosols, which were mainly apportioned to dust, were affected largely by aging processes, especially aqueous phase processes associated with RH higher than 70–80 %. Temporal variations in $Fe_{sol}$

https://doi.org/10.5194/egusphere-2026-3778
Preprint. Discussion started: 8 July 2026


concentrations were well correlated with those in BC concentrations, indicating the significance of continental combustion sources in enhancing $Fe_{sol}$ concentrations in the outflow regions. The $\Delta Fe_{sol}/\Delta BC$ were 53.8 (±11) ng $\mu g^{-1}$ on average during the observation period and increased from ~40 ng $\mu g^{-1}$ in winter to ~90 ng $\mu g^{-1}$ in spring, which could be reproduced by the IMPACT model. The modeled data analyses suggest that the observed seasonal changes in $\Delta Fe_{sol}/\Delta BC$ are primarily associated with the increase in the dust contribution to $Fe_{sol}$ in spring, and secondarily the larger contribution of the residential sector to BC compared to $Fe_{sol}$. Our observations provide combined datasets of size-segregated Fe and $Fe_{sol}$ concentrations and the evolution of $f_{Fe,sol}$ through aging processes as useful constraints to further develop, validate, and refine numerical models simulating the detailed behavior of Fe in aerosols over regions under East Asian winter monsoon influences.

## Data availability

All observation and model simulation data used in this study, except for the lidar observation datasets, will be available online (e.g., ZENODO). The data obtained from the MoEJ framework were downloaded from https://www.env.go.jp/air/osen/monitoring.html. The lidar observation datasets are available on the AD-Net website, hosted by the National Institute for Environmental Studies, Japan (https://www-lidar.nies.go.jp/AD-Net/).

## Author contributions

**Conceptualization:** T. M., A. I.; **Data curation:** T. M., C. Z., A. S., A. I.; **Formal analysis:** T. M.; **Funding acquisition:** T. M., A. I., Y. K.; **Investigation:** All authors; **Methodology:** T. M., A. I.; **Writing – original draft preparation:** T. M.; **Writing – review & editing:** All authors

## Competing interests

Y. K. is an editorial board member of Atmospheric Chemistry and Physics. A. I. is a co-organizer of an interjournal special issue of AMT/ACP/AR/BG "RUSTED: Reducing Uncertainty in Soluble aerosol Trace Element Deposition."

## Acknowledgements

This study was supported by JSPS KAKENHI (Grant No.: JP20H04329; JP23K11401), Specified Critical Technologies Research Promotion Grants from the Cabinet Office, Government of Japan, and Environmental Research and Technology Development Fund (Grant no.: JPMEERF20222001; JPMEERF20255001; JPMEERF24S12200) of the Environmental Restoration and Conservation Agency provided by the MoEJ. TM, CZ, and YK acknowledge H. Hayashi, M. Kubo, T. Takamura, and H. Irie (Chiba University) for their support at Fukue Island's Atmospheric Environment Monitoring Station.

https://doi.org/10.5194/egusphere-2026-3778
Preprint. Discussion started: 8 July 2026


AI acknowledges the JSPS KAKENHI Grant No. JP26K03081, Japan Science and Technology Agency (JST) Strategic International Collaborative Research Program (SICORP), Grant No. JPMJSC26A7, the Scientific Committee on Oceanic Research (SCOR) for their support of Working Group 167, Reducing Uncertainty in Soluble Aerosol Trace Element Deposition (RUSTED), via a grant to SCOR from the U.S. National Science Foundation (OCE-2513154) and the MEXT-Program for the advanced studies of climate change projection (SENTAN) Grant No. JPMXD0722681344. TM would like to thank Editage (https://www.editage.com/) for English language editing.

**References**

Al-Abadleh H. A., Kubicki, J, and Meshkhidze, N.: A perspective on iron (Fe) in the atmosphere: air quality, climate, and the ocean, Environ. Sci.: Processes Impacts, 25, 151–164, https://doi.org/10.1039/D2EM00176D, 2023.

Asano, H., Aoyama, T., Mizuno, Y., and Shiraishi, Y.: Highly time-resolved atmospheric observations using a continuous fine particulate matter and element monitor, ACS Ear. Spa. Chem., 1(9), 580–590, https://doi.org/10.1021/acsearthspacechem.7b00090, 2017.

Baker, A. R., Laskina, O., and Grassian, V. H.: Processing and Ageing in the Atmosphere, in: Mineral Dust: A Key Player in the Earth System, edited by: Knippertz, P. and Stuut, J.-B. W., Springer, Dordrecht, the Netherlands, 75–92, https://doi.org/10.1007/978-94-017-8978-3_4, 2014.

Basterretxea, G., Font-Muñoz, J. S., Hernández-Carrasco, I., and Sañudo-Wilhelmy, S. A.: Global variability of high-nutrient low-chlorophyll regions using neural networks and wavelet coherence analysis, Ocean Sci., 19, 973–990, https://doi.org/10.5194/os-19-973-2023, 2023.

Berger, C. J., Lippiatt, S. M., Lawrence, M. G., and Bruland, K. W.: Application of a chemical leach technique for estimating labile particulate aluminum, iron, and manganese in the Columbia River plume and coastal waters off Oregon and Washington, J. Geophys. Res., 113, C00B01, https://doi.org/10.1029/2007JC004703, 2008.

Brandt, C., and Van Eldik, R.: Transition Metal-Catalyzed Oxidation of Sulfur (IV) Oxides. Atmospheric-Relevant Processes and Mechanisms. Chem. Rev., *95* (1), 119–190, https://doi.org/10.1021/cr00033a006, 1995.

Buck, C. S., Landing, W. M., Resing, J. A., and Lebon, G. T.: Aerosol iron and aluminum solubility in the northwest Pacific Ocean: Results from the 2002 IOC cruise. Geochem. Geophy. Geosy., 7, Q04M07, https://doi.org/10.1029/2005GC000977, 2006.

Buck, C. S., Landing, W. M., Resing, J. A., and Measures, C. I.: The solubility and deposition of aerosol Fe and other trace elements in the North Atlantic Ocean: Observations from the A16N CLIVAR/CO2 repeat hydrography section, Mar. Chem., 120, 57–70, https://doi.org/10.1016/j.marchem.2008.08.003, 2010.

https://doi.org/10.5194/egusphere-2026-3778
Preprint. Discussion started: 8 July 2026


Buck, C. S., Landing, W. M., and Resing, J.: Pacific Ocean aerosols: Deposition and solubility of iron, aluminum, and other trace elements, Marine Chemistry, 157, 117–130, https://doi.org/10.1016/j.marchem.2013.09.005, 2013.

Cai Y., Irie H., Damiani A., Itahashi S., Takemura T., and Khatri P.: Detectability of the potential climate change effect on transboundary air pollution pathways in the downwind area of China, Sci Total Environ. 20;939: 173490. https://doi.org/10.1016/j.scitotenv.2024.173490, 2024.

Charrier, J. G., and Anastasio, C.: On dithiothreitol (DTT) as a measure of oxidative potential for ambient particles: evidence for the importance of soluble transition metals, Atmos. Chem. Phys., 12, 9321–9333, https://doi.org/10.5194/acp-12-9321-2012, 2012.

Chatani, S., Itahashi, S., and Yamaji, K.: Advantages of continuous monitoring of hourly PM2.5 component concentrations in Japan for model validation and source sensitivity analyses, Asi. J. Atmos. Environ., 15(2), 1-29, https://doi.org/10.5572/ajae.2021.008, 2021.

Chuang, P. Y., Duvall, R. M., Shafer, M. M., and Schauer, J. J.: The origin of water soluble particulate iron in the Asian atmospheric outflow, Geophys. Res. Lett., 32, L07813, https://doi.org/10.1029/2004GL021946, 2005.

Chow, J. C., Watson, J. G., Crow, D., Lowenthal, D. H., and Merrifield, T.: Comparison of IMPROVE and NIOSH carbon measurements, Aerosol Sci. Technol., 34, 23–34, https://doi.org/10.1080/02786820119073, 2001.

Chow, J. C., Watson, J. G., Chen, L.-W. A., Chang, M. C. O., Robinson, N. F., Trimble, D., and Kohl, S.: The IMPROVE_A temperature protocol for thermal/optical carbon analysis: maintaining consistency with a long-term database, J. Air Waste Manag. Assoc., 57, 1014–1023, https://doi.org/10.3155/1047-3289.57.9.1014, 2007.

Cosentino, N. J., Ruiz-Etcheverry, L. A., Bia, G.L., Simonella, L. E., Coppo, R., Torre, G., Saraceno, M., Tur, V. M., and Gaiero, D. M.: Does satellite chlorophyll-a respond to southernmost Patagonian dust? A multi-year, event-based approach. J. Geophys. Res.: Biogeosciences, 125, e2020JG006073. https://doi.org/10.1029/2020JG006073, 2020.

Cui, W., Song, X., Su, Y., Chen, X., Wu, D., and Li, Q.: Soluble iron in source-based anthropogenic $PM_{2.5}$ predominantly from steel industry and residential combustion in China, Geophys. Res. Lett., 52, e2025GL118603. https://doi.org/10.1029/2025GL118603, 2025.

Desboeufs, K., Formenti, P., Torres-Sánchez, R., Schepanski, K., Chaboureau, J.-P., Andersen, H., Cermak, J., Feuerstein, S., Laurent, B., Klopper, D., Namwoonde, A., Cazaunau, M., Chevaillier, S., Feron, A., Mirande-Bret, C., Triquet, S., and Piketh, S. J.: Fractional solubility of iron in mineral dust aerosols over coastal Namibia:

https://doi.org/10.5194/egusphere-2026-3778
Preprint. Discussion started: 8 July 2026


a link to marine biogenic emissions?, Atmos. Chem. Phys., 24, 1525–1541, https://doi.org/10.5194/acp-24-1525-2024, 2024.

Di Biagio, C., Balkanski, Y., Albani, S., Boucher, O., and Formenti, P.: Direct radiative effect by mineral dust aerosols constrained by new microphysical and spectral optical data, Geophys. Res. Lett., 47(2), 1–12. https://doi.org/10.1029/2019GL086186, 2020.

Dubois, N., Foret, G., Siour, G., Uzu, G., Couvidat, F., Vida, M., Andre, J.-M., Moukhtar, S., Sirina-Leboine, N., Aujay-Plouzeau, R., Alleman, L., Conil, S., Pallares, C., Salque-Moreton, G., Stratigou, E., Alastuey, A., Querol, X., Ito, A., Jaffrezo, J.-L., Favez, O., and Beekmann, M.: Construction of copper, iron and manganese anthropogenic emission inventories for Europe, Atmos. Envrion., 363, 15, 121582, https://doi.org/10.1016/j.atmosenv.2025.121582, 2025.

Hoesly, R., Smith, S., Ahsan, H., Prime, N., O'Rourke, P., Crippa, M., Klimont, Z., Guizzardi, D., Feng, L., Harkins, C., McDonald, B., and Wang, S.: CEDS v2025_04_18 gridded emissions data at 0.5° resolution, Zenodo [data set], https://doi.org/10.5281/zenodo.15127477, 2025.

Howell, S., Pszenny, A. A. P., Quinn, P., and Huebert, B.: A Field Intercomparison of Three Cascade Impactors, Aerosol Sci. Technol., 29(6), 475–492. https://doi.org/10.1080/02786829808965585, 1998.

Hsu S.-C., Wong G.T.F., Gong G.-C., Shiah F.-K., Huang Y.-T., Kao S.-J., Tsai F., Candice Lung S.-C., Lin F.-J., Lin I.I., Hung C.-C., and Tseng C.-M.: Sources, solubility, and dry deposition of aerosol trace elements over the East China Sea, Mar. Chem., 120, 116–127, https://doi.org/10.1016/j.marchem.2008.10.003, 2010.

Ito, A., and Kok, J. F.: Do dust emissions from sparsely vegetated regions dominate atmospheric iron supply to the Southern Ocean? J. Geophys. Res. Atmos., 122, 3987–4002, https://doi.org/10.1002/2016JD025939, 2017.

Ito, A., Lin, G., and Penner, J. E.: Radiative forcing by light-absorbing aerosols of pyrogenetic iron oxides. Sci. Rep., 8, 7347. https://doi.org/10.1038/s41598-018-25756-3, 2018.

Ito, A., Myriokefalitakis, S., Kanakidou, M., Mahowald, N. M., Scanza, R. A., Hamilton, D. S., Baker, A. R., Jickells, T., Sarin, M., Bikkina, S., and Gao, Y.: Pyrogenic iron: The missing link to high iron solubility in aerosols, Sci. Adv., 5(5), eaau7671, 2019.

Ito, A., Perron, M. M., Proemse, B. C., Strzelec, M., Gault-Ringold, M., Boyd, P. W., and Bowie, A. R.: Evaluation of aerosol iron solubility over Australian coastal regions based on inverse modeling: implications of bushfires on bioaccessible iron concentrations in the Southern Hemisphere, Prog. Earth Planet Sci., **7**, 42, https://doi.org/10.1186/s40645-020-00357-9, 2020.

Ito, A., Ye, Y., Baldo, C., and Shi, Z.: Ocean fertilization by pyrogenic aerosol iron, Npj Clim. Atmos. Sci. 4, 30. https://doi.org/10.1038/s41612-021-00185-8, 2021.

https://doi.org/10.5194/egusphere-2026-3778
Preprint. Discussion started: 8 July 2026


Ito, A. and Miyakawa, T.: Aerosol Iron from Metal Production as a Secondary Source of Bioaccessible Iron, Environ. Sci. Tech., 57(10), 4091–4100, https://doi.org/10.1021/acs.est.2c06472, 2023.

Ito, A., Miyazaki, Y., Taketani, F., Iwamoto, Y., and Kanaya, Y.: Marine aerosol feedback on biogeochemical cycles and the climate in the Anthropocene: lessons learned from the Pacific Ocean, Environ. Sci.: Atmos., https://doi.org/10.1039/D2EA00156J, 2023.

Jeong, G. Y.: Mineralogy and geochemistry of Asian dust: dependence on migration path, fractionation, and reactions with polluted air, Atm. Chem. Phys., 20, 7411–7428, https://doi.org/10.5194/acp-20-7411-2020, 2020.

Jickells, T. D., An, Z. S., Andersen, K. K., Baker, A. R., Bergametti, G., Brooks, N., Cao, J. J., Boyd, P. W., Duce, R. A., Hunter, K. A., Kawahata, H., Kubilay, N., laRoche, J., Liss, P. S., Mahowald, N., Prospero, J. M., Ridgwell, A. J., Tegen, I., and Torres, R.: Global iron connections between desert dust, ocean biogeochemistry, and climate, Science, 1; 308 (5718): 67–71. https://doi.org/ 10.1126/science.1105959, 2005.

Johnson, M. S. and Meskhidze, N.: Atmospheric dissolved iron deposition to the global oceans: effects of oxalate-promoted Fe dissolution, photochemical redox cycling, and dust mineralogy, Geosci. Model Dev., 6, 1137–1155, https://doi.org/10.5194/gmd-6-1137-2013, 2013.

Jordi, A., Basterretxea, G., Tovar-Sanchez, A., Alastuey, A., and Querol, X.: Copper aerosols inhibit phytoplankton growth in the Mediterranean Sea, Proc. Nat. Aca. Sci., 109(52), 21246–21249, https://doi.org/10.1073/pnas.1207567110, 2012, 2012.

Kajino, M., Hagino, H., Fujitani, Y., Morikawa, T., Fukui, T., Onishi, K., Okuda, T., Kajikawa, T., and Igarashi, Y.: Modeling transition metals in East Asia and Japan and its emission sources, GeoHeath, 4, e2020GH000259. https://doi.org/10.1029/2020GH000259, 2020.

Kajino, M., Hagino, H., Fujitani, Y., Morikawa, T., Fukui, T., Onishi, K., Okuda, T., and Igarashi, Y.: Simulation of the transition metal-based cumulative oxidative potential in East Asia and its emission sources in Japan. Sci. Rep., 11, 6550. https://doi.org/10.1038/s41598-021-85894-z, 2021.

Kanaya, Y., Pan, X., Miyakawa, T., Komazaki, Y., Taketani, F., Uno, I., and Kondo, Y.: Long-term observations of black carbon mass concentrations at Fukue Island, western Japan, during 2009–2015: constraining wet removal rates and emission strengths from East Asia, Atmos. Chem. Phys., 16, 10689–10705, https://doi.org/10.5194/acp-16-10689-2016, 2016.

Kanaya, Y., Yamaji, K., Miyakawa, T., Taketani, F., Zhu, C., Choi, Y., Komazaki, Y., Ikeda, K., Kondo, Y., and Klimont, Z.: Rapid reduction in black carbon emissions from China: evidence from 2009–2019 observations on Fukue Island, Japan, Atmos. Chem. Phys., 20, 6339–6356, https://doi.org/10.5194/acp-20-6339-2020, 2020.

https://doi.org/10.5194/egusphere-2026-3778
Preprint. Discussion started: 8 July 2026


Kanaya, Y., Yamaji, K., Miyakawa, T., Taketani, F., Zhu, C., Choi, Y., Ikeda, K., Tanimoto, H., Yamada, D., Narita, D., and Kondo, Y.: Dominance of the residential sector in Chinese black carbon emissions as identified from downwind atmospheric observations during the COVID-19 pandemic, Sci. Rep., 11, 23378, https://doi.org/10.1038/s41598-021-02518-2, 2021.

Karydis, V. A., Kumar, P., Barahona, D., Sokolik, I. N., and Nenes, A.: On the effect of dust particles on global cloud condensation nuclei and cloud droplet number, J. Geophys. Res., 116, D23204, https://doi.org/10.1029/2011JD016283, 2011.

Kenny, L. C., Merrifield, T., Mark, D., Gussman, R., and Thorpe, A.: The development and designation testing of a New EPA approved fine particle inlet: A study of the U.S. EPA designation process, *Aerosol Sci. Tech.*, 38:15–22, https://doi.org/10.1080/027868290502290, 2004.

Kok, J. F., Adebiyi, A. A., Albani, S., Balkanski, Y., Checa-Garcia, R., Chin, M., Colarco, P. R., Hamilton, D. S., Huang, Y., Ito, A., Klose, M., Li, L., Mahowald, N. M., Miller, R. L., Obiso, V., Perez Garcia-Pando, C., Rocha-Lima, A., and Wan, J. S.: Contribution of the world's main dust source regions to the global cycle of desert dust, Atmos. Chem. Phys., 21, 8169–8193, https://doi.org/10.5194/acp-21-8169-2021, 2021.

Kurisu, M., Sakata, K., Uematsu, M., Ito, A., and Takahashi, Y.: Contribution of combustion Fe in marine aerosols over the northwestern Pacific estimated by Fe stable isotope ratios, Atmos. Chem. Phys., 21, 16027–16050, https://doi.org/10.5194/acp21-16027-2021, 2021.

Kurisu, M., Zhu, C., Miyakawa, T., Ito, A., Suzuki, K., Kashiwabara, T., Kubo, S., Takahashi, Y., Harada, N., Foret, G., Dubois, N., and Kanaya, Y.: Identification of anthropogenic Fe originated from East Asia using Fe stable isotope ratios of aerosols collected on Fukue Island, Atmos. Environ., 373, 15, https://doi.org/10.1016/j.atmosenv.2026.121893, 2026.

Lakey, P. S., Berkemeier, T., Tong, H., Arangio, A. M., Lucas, K., Pöschl, U., and Shiraiwa, M.: Chemical exposure-response relationship between air pollutants and reactive oxygen species in the human respiratory tract, Sci. Rep. 6, 32916; https://doi.org/10.1038/srep32916, 2016.

Lamb, K. D., Matsui, H., Katich, J. M., Perring, A. E., Spackman, J. R., Weinzierl, B., Dollner, M., and Schwarz, J. P.: Global-scale constraints on light-absorbing anthropogenic iron oxide aerosols, Npj Clim. Atmos. Sci 4, 15. https://doi.org/10.1038/s41612-021-00171-0, 2021.

Li, R., Plaas, H. E., Zhang, Y., Chen, Y., Zhang, T., Yang, Y., Rathod, S., Zhang, G., Wang, X., Hamilton, D. S., and Tang, M.: Residential burning is a significant source of soluble iron to the ocean, Atmos. Chem. Phys., 26, 9037–9060, https://doi.org/10.5194/acp-26-9037-9060, 2026.

https://doi.org/10.5194/egusphere-2026-3778
Preprint. Discussion started: 8 July 2026


Mahowald, N. M., Hamilton, D. S., Mackey, K. R, Moore, J. K., Baker, A. R., Scanza, R. A., and Zhang, Y.: Aerosol trace metal leaching and impacts on marine microorganisms. Nat. Commun. 9, 2614. https://doi.org/10.1038/s41467-018-04970-7, 2018.

McCoy, D. T., Bender, F. M., Mohrmann, J. K. C., Hartmann, D. L., Wood, R., and Grosvenor, D. P.: The global aerosol-cloud first indirect effect estimated using MODIS, MERRA, and AeroCom. J. Geophys. Res. Atmos., 122, 1779–1796, doi:10.1002/2016JD026141, 2017.

Meskhidze, N., Hamilton, D., Perron, M., and Ito, A.: From Dust to Phytoplankton: Research Priorities for Atmospheric-Ocean Iron Coupling. Zenodo., https://doi.org/10.5281/zenodo.19361638, 2026.

Miyakawa, T., Oshima, N., Taketani, F., Komazaki, Y., Yoshino, A., Takami, A., Kondo, Y., and Kanaya, Y.: Alteration of the size distributions and mixing states of black carbon through transport in the boundary layer in East Asia, Atmos. Chem. Phys., 17, 5851–5864, https://doi.org/10.5194/acp-17-5851-2017, 2017.

Miyakawa, T., Komazaki, Y., Zhu, C., Taketani, F., Pan, X., Wang, Z., and Kanaya, Y.: Characterization of carbonaceous aerosols in Asian outflow in the spring of 2015: importance of non-fossil fuel sources, Atmos. Environ., 214, 116858, https://doi.org/10.1016/j.atmosenv.2019.116858, 2019.

Miyakawa, T., Mordovskoi, P., and Kanaya, Y.: Evaluation of black carbon mass concentrations measured using a miniaturized aethalometer in comparison with continuous soot monitoring system (COSMOS) and single-particle soot photometer (SP2), Aerosol Sci. Technol., 54:7, 811–825, https://doi.org/10.1080/02786826.2020.1724870, 2020.

Miyakawa, T., Ito, A., Zhu, C., Shimizu, A., Matsumoto, E., Mizuno, Y., and Kanaya, Y.: Trace elements in PM2.5 aerosols in East Asian outflow in the spring of 2018: Emission, transport, and source apportionment, Atmos. Chem. Phys., 23, 14609–14626, https://doi.org/10.5194/acp-23-14609-2023, 2023.

Miyakawa, T., Kinase, T., Kurisu, M., Taniguchi, K., Katsumata, M., Takashima, H., Taketani, F., and Kanaya, Y.: Natural and continental influence on aerosol distributions over the Northwestern Pacific Ocean in the late winter and early spring of 2021, Prog. Earth Planet. Sci., 12, 77, https://doi.org/10.1186/s40645-025-00752-0, 2025.

Moore, C., Mills, M., Arrigo, K. R., Berman-Frank, I., Bopp, L., Boyd, P. W., Galbraith, E. D., Geider, R. J., Guieu, C., Jaccard, S. L., and Jickells, T. D.: Processes and patterns of oceanic nutrient limitation, Nature Geosci 6, 701–710. https://doi.org/10.1038/ngeo1765, 2013.

Moteki, N., Kondo, Y., Oshima, N., Takegawa, N., Koike, M., Kita, K., Matsui, H., and Kajino, M.: Size dependence of wet removal of black carbon aerosols during transport from the boundary layer to the free troposphere, Geophys. Res. Lett., 39, L13802, https://doi.org/10.1029/2012GL052034, 2012.

https://doi.org/10.5194/egusphere-2026-3778
Preprint. Discussion started: 8 July 2026


Myhre, G., Myhre, C. L., Samset, B. H., and Storelvmo, T.: Aerosols and their relation to global climate and climate sensitivity, Nat. Educ. Knowl., 4, 7, 2013.

Myriokefalitakis, S., Daskalakis, N., Mihalopoulos, N., Baker, A. R., Nenes, A., and Kanakidou, M.: Changes in dissolved iron deposition to the oceans driven by human activity: a 3-D global modelling study, Biogeosciences, 12, 3973–3992, https://doi.org/10.5194/bg-12-3973-2015, 2015.

Nagashima, K., Kawakami, H., Sugie, K., Fujiki, T., Nishioka, J., Iwamoto, Y., Takemura, T., Miyakawa, T., Taketani, F., and Aita, M. N.: Asian dust-deposition flux to the subarctic Pacific estimated using single quartz particles, Sci. Rep. 13, 15424, https://doi.org/10.1038/s41598-023-41201-6, 2023.

Nenes, A., Murray, B., and Bougiatioti, A.: Mineral dust and its microphysical interactions with clouds, in: Mineral Dust: A Key Player in the Earth System, edited by: Knippertz, P. and Stuut, J.-B. W., Springer, Dordrecht, the Netherlands, 287–325, https://doi.org/10.1007/978-94-017-8978-3_12, 2014.

Pacyna, J. M. and Pacyna, E. G.: An assessment of global and regional emissions of trace metals to the atmosphere from anthropogenic sources worldwide, Environ. Rev., 9, 269–298, https://doi.org/10.1139/a01-012, 2001.

Paris, R. and Desboeufs, K. V.: Effect of atmospheric organic complexation on iron-bearing dust solubility, Atmos. Chem. Phys., 13, 4895–4905, https://doi.org/10.5194/acp-13-4895-2013, 2013.

Perron, M. M., Strzelec, M., Gault-Ringold, M., Proemse, B. C., Boyd, P. W., and Bowie, A. R.: Assessment of leaching protocols to determine the solubility of trace metals in aerosols, Talanta, 208, 120377, https://doi.org/10.1016/j.talanta.2019.120377, 2020.

Sakata, K., Takano, S., Matsuki, A., Takeichi, Y., Tanimoto, H., Sakaguchi, A., Kurisu, M., and Takahashi, Y.: Atmospheric chemistry in East Asia determines the iron solubility of aerosol particles supplied to the North Pacific Ocean, Atmos. Chem. Phys., 25, 11087–11107, https://doi.org/10.5194/acp-25-11087-2025, 2025.

Sayer, A. M., Munchak, L. A., Hsu, N. C., Levy, R. C., Bettenhausen, C., and Jeong, M.-J.: MODIS Collection 6 aerosol products: Comparison between Aqua's e-Deep Blue, Dark Target, and "merged" data sets, and usage recommendations, J. Geophys. Res. Atmos., 119, 13965–13989, https://doi.org/10.1002/2014JD022453, 2014.

Scanza, R. A., Hamilton, D. S., Pérez García-Pando, C., Buck, C., Baker, A. R., and Mahowald, N. M.: Atmospheric processing of iron in mineral and combustion aerosols: development of an intermediate-complexity mechanism suitable for Earth system models, Atmos. Chem. Phys., 18, 14175–14196, https://doi.org/10.5194/acp-18-14175-2018, 2018.

Schauer, J. J., Mader, B. T., DeMinter, J. T., Heidemann, G., Bae, M. S., Seinfeld, J. H., Flagan, R. C., Cary, R. A., Smith, D., Huebert, B. J., Bertram, T., Howell, S., Kline, J. T., Quinn, P., Bates, T., Turpin, B., Lim, H. J., Yu, J. Z., Yang, H., and Keywood, M. D.: ACE-Asia intercomparison of a thermal-optical method for the

https://doi.org/10.5194/egusphere-2026-3778
Preprint. Discussion started: 8 July 2026


determination of particle-phase organic and elemental carbon, Environ. Sci. Technol., 37, 993–1001, https://doi.org/10.1021/es020622f, 2003.

Shelley, R. U., Landing, W. M., Ussher, S. J., Planquette, H., and Sarthou, G.: Regional trends in the fractional solubility of Fe and other metals from North Atlantic aerosols (GEOTRACES cruises GA01 and GA03) following a two-stage leach, Biogeo., 15, 2271–2288, https://doi.org/10.5194/bg-15-2271-2018, 2018.

Shi, Z., Krom, M. D., Bonneville, S., and Benning, L. G.: Atmospheric Processing Outside Clouds Increases Soluble Iron in Mineral Dust, Environ. Sci. Technol., 49 (3), 1472–1477, https://doi.org/10.1021/es504623x, 2015.

Shi, J., Guan, Y., Ito, A., Gao, H., Yao, X., Baker, A. R., and Zhang, D.: High production of soluble iron promoted by aerosol acidification in fog, Geophys. Res. Lett., 47, e2019GL086124, https://doi.org/10.1029/2019GL086124, 2020.

Shimizu, A., Sugimoto, N., Matsui, I., Arao, K., Uno, I., Murayama, T., Kagawa, N., Aoki, K., Uchiyama, A., and Yamazaki, A.: Continuous observations of Asian dust and other aerosols by polarization lidar in China and Japan during ACE-Asia, J. Geophys. Res., 109, D19S17, https://doi.org/10.1029/2002JD003253, 2004.

Shimizu, A., Sugimoto, N., Matsui, I., Mori, I., Nishikawa, M., and Kido, M.: Relationship between lidar-derived dust extinction coefficients and mass concentrations in Japan, SOLA, 7A, 1–4, https://doi.org/10.2151/sola.7A-001, 2011.

Shimizu, A., Nishizawa, T., Jin, Y., Kim, S. W., Wang, Z., Batdorj, D., and Sugimoto, N.: Evolution of a lidar network for tropospheric aerosol detection in East Asia, Opt. Eng., 56, 3, 031219, https://doi.org/10.1117/1.OE.56.3.031219, 2016.

Sholkovitz, E. R., Sedwick, P. N., Church, T. M., Baker, A. R., and Powell, C. F.: Fractional solubility of aerosol iron: Synthesis of a global-scale dataset, Geochim. Cosmochim. Ac, 89, 173–189, https://doi.org/10.1016/j.gca.2012.04.022, 2012.

Stein, A. F., Draxler, R. R., Rolph, G. D., Stunder, B. J. B., Cohen, M. D., and Ngan, F.: NOAA's HYSPLIT atmospheric transport and dispersion modeling system, Bull. Am. Meteorol. Soc. 96, 2059–2077. https://doi.org/10.1175/BAMS-D-14-00110.1, 2015.

Sugimoto, N., Uno, I., Nishikawa, M., Shimizu, A., Matsui, I., Dong, X., Chen, Y., and Quan, H.: Record heavy Asian dust in Beijing in 2002: observations and model analysis of recent events, Geophys. Res. Lett., 30, 1640, https://doi.org/10.1029/2002GL016349, 2003.

Tagliabue, A., Bowie, A. R., Boyd, P. W., Buck, K. N., Johnson, K. S., and Saito, M. A.: The integral role of iron in ocean biogeochemistry, Nature, 543, 51–59. https://doi.org/10.1038/nature21058, 2017.

https://doi.org/10.5194/egusphere-2026-3778
Preprint. Discussion started: 8 July 2026


Tang, M., Perron, M. M., Baker, A. R., Li, R., Bowie, A. R., Buck, C. S., Kumar, A., Shelley, R., Ussher, S. J., Clough, R., Meyerink, S., Panda, P. P., Townsend, A. T., and Wyatt, N.: Measurement of soluble aerosol trace elements: inter-laboratory comparison of eight leaching protocols, Atmos. Meas. Tech., 18, 6125–6141, https://doi.org/10.5194/amt-18-6125-2025, 2025.

Tegen, I. and Lacis, A. A.: Modeling of particle size distribution and its influence on the radiative properties of mineral dust aerosol, J. Geophys. Res., 101(D14), 19237–19244, https://doi.org/10.1029/95JD03610, 1996.

Wang, Q., Zhuang, G., Li, J., Huang, K., Zhang, R., Jiang, Y., Lin, Y., and Fu, J. S.: Mixing of dust with pollution on the transport path of Asian dust – revealed from the aerosol over Yulin, the north edge of Loess Plateau, Sci. Tot. Environ., 409(3), 573–581, https://doi.org/10.1016/j.scitotenv.2010.10.032, 2011.

Willeke, K.: Performance of the slotted impactor, Am. Ind. Hyg. Assoc. J., 36, 683–691, https://doi.org/10.1080/0002889758507315, 1975.

Wu, C., Lin, Z., Shao, Y., Liu, X., and Li, Y.: Drivers of recent decline in dust activity over East Asia. Nat. Commun., 13, 7105, https://doi.org/10.1038/s41467-022-34823-3, 2022.

Xie, Y., Zeng, L., Hu, S., Wang, T., Du, Z., Tan, T., Xu, N., Chen, S., Mao, J., Xu, F., and Hu, M.: Long-term trends of black carbon levels, sources, and radiative effects from 2013 to 2022 in Beijing, China, npj Clean Air, 1, 10, https://doi.org/10.1038/s44407-025-00010-z, 2025.

Zhu, Y., Li, W., Lin, Q., Yuan, Q., Liu, L., Zhang, J., Zhang, Y., Shao, L., Niu, H., Yang, S., and Shi, Z.: Iron solubility in fine particles associated with secondary acidic aerosols in east China, Environ. Pollut., 264, 114769, https://doi.org/10.1016/j.envpol.2020.114769, 2020.

Zhu, C., Miyakawa, T., Irie, H., Choi, Y., Taketani, F., and Kanaya, Y.: Light-absorption properties of brown carbon aerosols in the Asian outflow: Implications of a combination of filter and ground remote-sensing observations at Fukue Island, Japan, Sci. Tot. Environ., 797, 149155, https://doi.org/10.1016/j.scitotenv.2021.149155, 2021.

Zhu, H., Liu, Y., Yue, M., Feng, S., Fu, P., Huang, K., Dong, X., and Wang, M.: Trends and drivers of soluble iron deposition from East Asian dust to the Northwest Pacific: a springtime analysis (2001–2017), Atmos. Chem. Phys., 25, 5175–5197, https://doi.org/10.5194/acp-25-5175-2025, 2025.